PERGAMON

Journal of Structural Geology 23 (2001) 1255–1279

JOURNAL OF STRUCTURAL GEOLOGY

www.elsevier.nl/locate/jstrugeo

Paleomagnetic data bearing on style of Miocene deformation in the Lake Mead area, southern Nevada

Tim F. Wawrzyniec[a,*], John W. Geissman[a], R. Ernest Anderson[b], Steve S. Harlan[a,1], James Faulds[a,2]

[a]*Department of Earth and Planetary Sciences, University of New Mexico, Albuquerque, NM 87131-1116, USA*
[b]*US Geological Survey, MS 966, Box 25046, Denver Federal Center, Denver, CO 80225, USA*

Received 22 February 1999; accepted 21 November 2000

Abstract

Paleomagnetic and structural data from intermediate to mafic composition lava flows and related dikes in all major blocks of the late Miocene Hamblin–Cleopatra Volcano, which was structurally dismembered during the development of the Lake Mead Fault System (LMFS), provide limits on the magnitude and sense of tilting and vertical axis rotation of crust during extension of this part of the Basin and Range province. Sinistral separation along the fault system dissected the volcano into three major blocks. The eastern, Cleopatra Lobe of the volcano is structurally the most intact section of the volcano. Normal and reverse polarity data from paleomagnetic sites collected along traverses in the Cleopatra Lobe yield an in situ grand mean of Declination (D) = 339°, Inclination (I) = +54°, $\alpha_{95} = 3.1°$, $k = 27.2$, $N = 81$ sites. The rocks of the central core of the volcano yield an in situ grand mean of $D = 3°$, $I = +59°$, $\alpha_{95} = 6.8°$, $k = 42.5$, $N = 11$ sites (six normal, five reverse polarity). Sites collected within the western Hamblin Lobe of the volcano are exclusively of reverse polarity and yield an overall in situ mean of $D = 168°$, $I = -58°$, $\alpha_{95} = 6.5°$, $k = 28.9$, $N = 18$ sites. Interpretation of the paleomagnetic data in the context of the structural history of the volcano and surrounding area, considers the possibility of two different types of structural corrections. A stratigraphic tilt correction involves restoring flows to the horizontal using the present strike. This correction assumes no initial, possibly radial, dip of flows of the volcano and is considered invalid. A structural tilt correction to the data assumes that dikes of the radiating swarm associated with the volcano were originally vertical and results in block mean directions of $D = 9°$, $I = +53°$, $\alpha_{95} = 3.1°$, $k = 27.2$, and $D = 58°$, $I = +78°$, $\alpha_{95} = 6.8°$, $k = 42.5$, for the Cleopatra Lobe and the central intrusive core, respectively. The data from the Cleopatra Lobe are slightly discordant, in a clockwise sense, from expected middle- to late-Miocene field directions. The data from the volcano are not consistent with a proposed structural model of uniform, moderate magnitude, statistically significant, counter-clockwise vertical axis rotation of fault-bounded blocks during overall sinsitral displacement along the LMFS. We also analyzed dikes of the northernmost part of the Miocene Wilson Ridge hypabyssal igneous complex, strata of the Triassic Chinle Formation, and basalt flows of the Miocene West End Wash/Callville Mesa volcanic centers. Dikes in the Wilson Ridge pluton and the Triassic strata yield magnetizations with directions suggestive of statistically significant, clockwise, vertical-axis rotations consistent with local, large-magnitude shear of crustal fragments near some of the faults of the LMFS. Late Cenozoic deformation of the Hamblin–Cleopatra volcano area appears to have been non-uniform in scale and magnitude and no single structural model, involving strictly strike-slip faulting, can account for the observed paleomagnetic data.

Keywords: Basin and Range province; Miocene; Paleomagnetism; Rotation; Strike-slip faults

1. Introduction and geology

Assessing the degree of tilt and vertical axis rotation of brittly deformed rocks is perhaps the most direct way to evaluate the relative importance of strike-slip or dip-slip shear zones as structures accommodating a large-scale extension in the continental lithosphere. In the context of well-documented field relations, paleomagnetism can provide a quantitative assessment of finite tilts or rotations associated with deformation that post-dates remanent magnetization acquisition (e.g. Faulds et al., 1992; Sonder et al., 1994). Within the Basin and Range province, at the latitude of Lake Mead, southern Nevada, continental lithosphere extension is characterized by several large

* Corresponding author. Present address: Bureau of Economic Geology, University of Texas at Austin, University Station, Box X, Austin, TX 78713-8924, USA.

E-mail address: tim.wawrzyniec@beg.utexas.edu (T.F. Wawrzyniec).

[1] Current address: Department of Geography and Earth Sciences, George Mason University, Fairfax, VA 22030, USA.

[2] Current address: Nevada Bureau of Mines and Geology, University of Nevada, Reno, NV 89557, USA.

0191-8141/01/$ - see front matter
PII: S0191-8141(00)00191-7

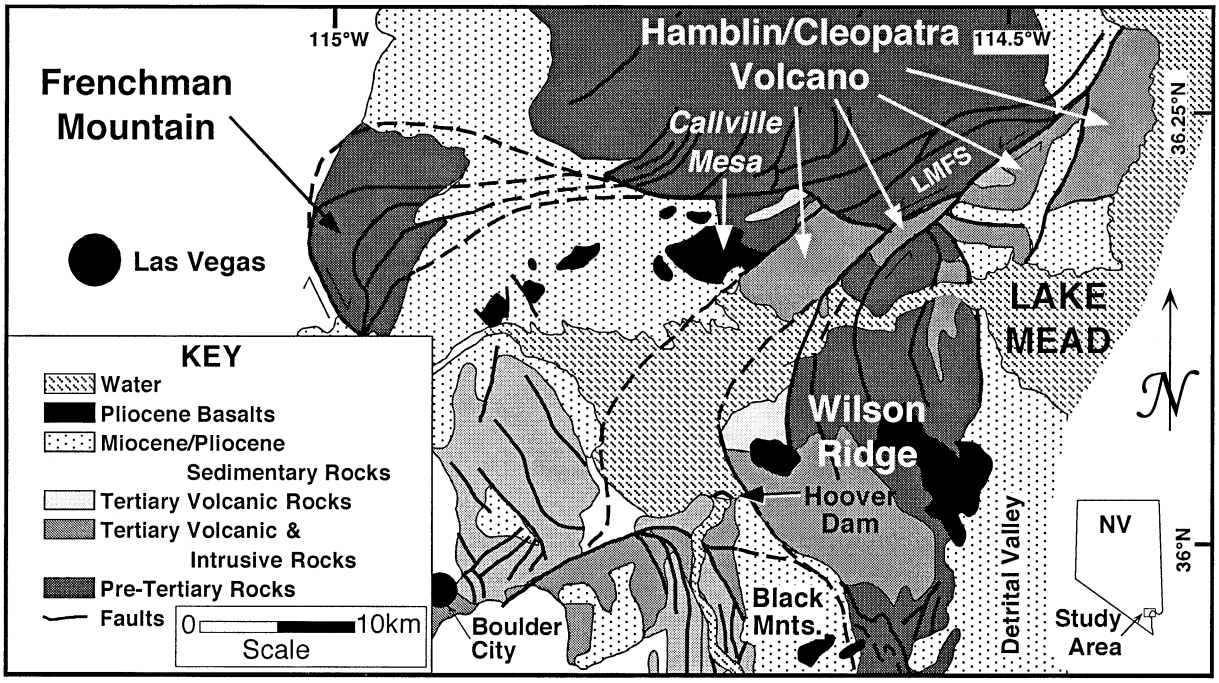

Fig. 1. Generalized regional geologic map of the northern end of the Colorado River extensional corridor, southern Nevada. The faulted and offset Hamblin–Cleopatra Volcano is exposed along the southwest part of the Lake Mead Fault System (LMFS). Adapted from Angelier et al. (1985).

strike-slip faults. Major structures include the NW-striking Las Vegas Valley shear zone, with an estimated dextral displacement of 48 km (Longwell, 1950, 1974; Burchfiel 1965; Fleck, 1970; Wernicke et al., 1988), and the NE-striking Lake Mead Fault System (LMFS), with an estimated sinistral displacement of 65 km (Anderson, 1973; Bohannon, 1979, 1984). Within the Lake Mead area (Fig. 1), faulting during the Neogene has long been recognized as having been dominated by coeval strike-slip and dip-slip structures (Anderson, 1973). There is still no general agreement, however, on how the two types of faults interact or which type serves as the dominant, first-order structure accommodating the bulk of extension in this part of the province. Fortunately, extension in this area is at least locally associated with syn-tectonic volcanic and intrusive rocks that are well-suited for paleomagnetic analysis. We report the results of a paleomagnetic study of rocks comprising, or spatially associated with, the mid-Miocene Hamblin–Cleopatra Volcano, which is a pre- to syn-tectonic volcanic feature deformed by both strike-slip and dip-slip faults of the LMFS. We discuss the bearing of these results on the relative role of strike-slip versus dip-slip faults in the extension of continental lithosphere affected by slip along the LMFS.

The Hamblin–Cleopatra Volcano, about 60 km^3 in volume, is composed of lava flows, flow breccias and interstratified volcaniclastic rocks of mafic intermediate chemical composition (Anderson, 1973) that have been reported to be suitable for paleomagnetic study (Ron et al., 1986). Many of these rocks are cut by syn-volcanic dikes, sills, and small intrusive plugs that are locally associated with contact aureoles of variable width or degree of contact metamorphism. The maximum cumulative thickness of associated volcanic products approaches 1 km. A laterally continuous disconformable contact within the volcanic sequence records two phases of shield-building activity with a brief hiatus in volcanism (Thompson, 1985). Whole rock K–Ar age determinations that range from 12.7 (±0.8) to 11.3 (±0.3) Ma (Anderson et al., 1972) indicate volcanic activity between 13 and 11 Ma (Anderson et al., 1972; Bohannon, 1984; Thompson, 1985). Additional whole rock $^{40}Ar/^{39}Ar$ age spectrum data (Anderson et al., 1994) range from 11.71 to 10.07 Ma. Strike-slip faulting has resulted in separation of the composite volcano into three main lobes referred to by Anderson et al. (1994) as the Hamblin Mountain, middle and Cleopatra Wash Lobes. Herein, these are referred to as the Hamblin (western), middle and Cleopatra (eastern) Lobes (Fig. 2). A distinction made here, based on the mapping of Anderson (1973), is a fourth part to the volcano—the central intrusive complex. The central intrusive complex is composed of mafic- to intermediate-intrusive and extrusive rocks thought to have once been associated with a central cone that was subsequently dissected by post- and possibly syn-eruptive faulting (Anderson, 1973; Anderson et al., 1994). Each of the three flow-dominated lobes is deeply eroded (Fig. 3) and exposes up to 900 m of interbedded volcaniclastic deposits and lavas that lie on about 200 m of interstratified basaltic lavas and associated detrital sedimentary strata. Incised canyons provide excellent exposures of the radial dike swarm, including the central core where the dikes make up about 80% of the exposed igneous rock (Anderson, 1973).

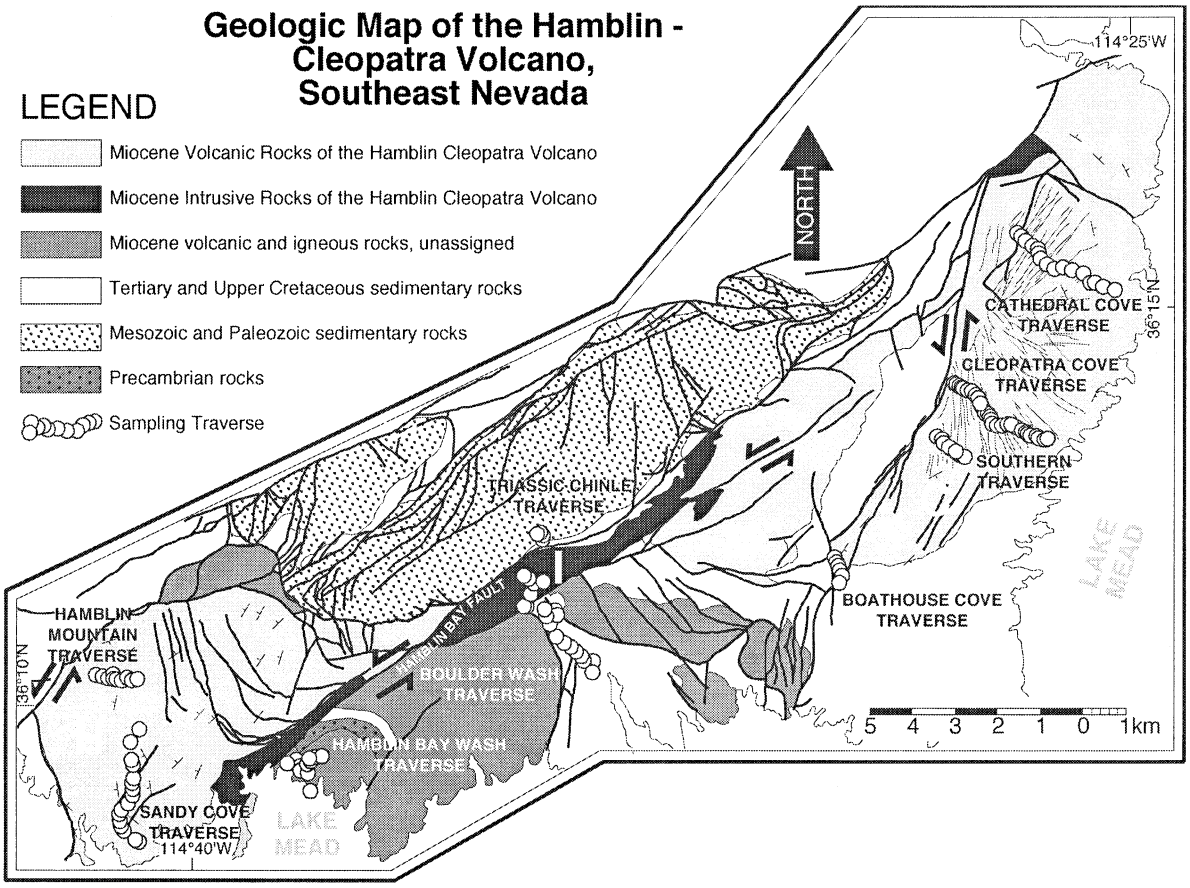

Fig. 2. Geologic map of the Hamblin–Cleopatra Volcano, showing the locations of sampling traverses (summarized in Table 1). The principal displacements on faults of the Lake Mead Fault System are sinistral. The Hamblin Lobe, Middle Lobe, Intrusive core and Cleopatra Lobe are labeled H, M, I and C, respectively. The lobes of the volcano are offset principally along the Hamblin Bay Fault (redrawn from Anderson (1973)).

The volcano lies on the boundary between the Great Basin sector of the Basin and Range province (Eaton, 1978) and the lower Colorado River extensional corridor (John and Howard, 1994). This boundary is marked by the left-lateral LMFS, strands of which cut the volcano into its three main lobes and have offsets as high as 20 km (Anderson, 1973). In addition, the volcano and related rocks lie in the upper plate of a regionally-extensive west-dipping detachment fault system, the trace of which lies on the west flank of the South Virgin Mountains (Duebendorfer et al., 1998). The dissection of the volcano into internally coherent lobes makes it ideal for applying paleomagnetism to evaluate possible mechanisms of strike-slip and dip-slip faulting (Fig. 4) in attending steep-axis rotation and/or tilting during middle Miocene and younger extension.

In addition to the rocks of the volcano, we collected rocks that are either spatially or temporally associated with the eruptive complex. The Hamblin lobe of the volcano is in fault contact with hypabyssal intrusions of the northernmost part of the middle Miocene (ca. 13.5 Ma for main intrusions and ca. 12.6 Ma for hypabyssal dikes) Wilson Ridge pluton, which is interpreted as an extensional dike-on-dike complex that extends at least 5 km south of Lake Mead (Anderson and Barnhard, 1991; Metcalf and Smith, 1991; Anderson et al., 1994). Structural evidence and map patterns suggest that strain partitioning across the Hamblin Bay Fault resulted in counterclockwise bending, about a sub-vertical axis, of Wilson Ridge dikes with essentially no consistent flexure of Hamblin Lobe rocks to the northwest. This has been attributed to depth-variable distribution of strain, associated decoupling, and syn-extensional north–south shortening (Anderson and Barnhard, 1991; Anderson et al., 1994). Sites were also established in nearly flat-lying flows of the Miocene West End Wash/Callville Mesa volcanic centers and in tilted strata of the Triassic Chinle Formation. Although the latter are much older than the volcano, these rocks are part of a large block that may have experienced rotation in association with slip along the LMFS. Basaltic to basaltic–andesite flows of the West End Wash/Callville Mesa volcanic centers in the Callville Mesa area have yielded K/Ar dates on groundmass plagioclase from 10.46 (±0.23) to 8.49 (±0.20) Ma (Feuerbach et al., 1991). A basaltic–andesite flow, collected 5 km west of Callville Mesa, has been dated by $^{40}Ar/^{39}Ar$ whole rock methods to be 11.41 ± 0.14 (2σ) Ma (Harlan et al., 1998). This age determination, if the rock is correlative with the Callville Mesa/West End Wash centers, implies eruption during and/or prior to the dissection of the

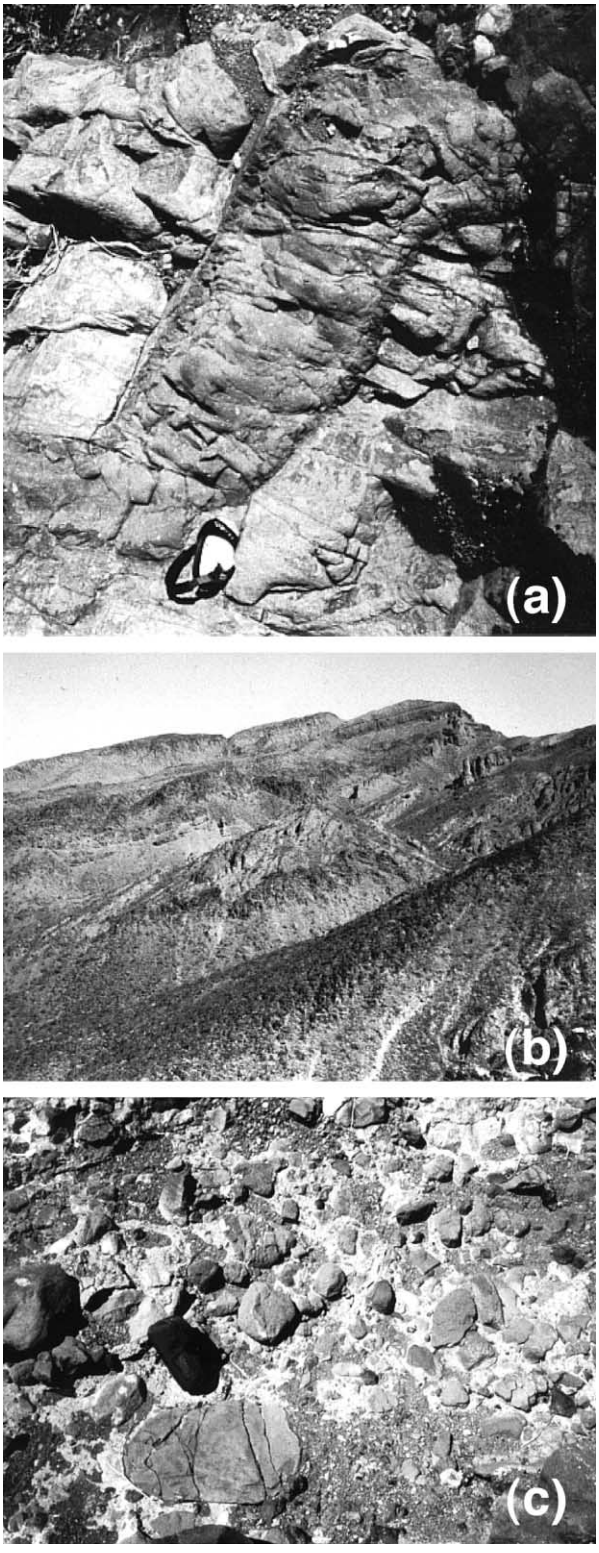

Fig. 3. Photographs of different volcanic sequences/intrusions exposed along drainages that dissect the Hamblin–Cleopatra Volcano. (a) Sub-vertical mafic dike (25–35 cm wide) located at site HC52, (b) typical sequence of volcaniclastic deposits and lava flows of the Cleopatra Lobe (view is approximately 2 km wide), (c) volcanic breccia sampled at site SC60, located at the west end of the Sandy Cove Traverse of the Hamblin Lobe (long axis of the large clast in the lower half of the photograph is approximately 40 cm; results of a conglomerate test at this site are summarized in Fig. 7).

Hamblin–Cleopatra Volcano. Therefore, these rocks may also record some degree of rotation and/or tilting in faulting along the LMFS.

Paleomagnetism is a powerful tool in quantifying components of deformation in many structural settings, but the approach has limitations. To assess absolute vertical-axis rotations, paleomagnetic studies require: (1) definition of discrete coherent structural blocks, (2) either a data set from each coherent block that has sufficiently averaged paleosecular variation (in order for comparison with expected directions derived from apparent polar wander path data) or a single, laterally extensive deposit with a uniform magnetization (in order to infer relative rotations), and (3) a magnetization characteristic of each coherent block that is accurately referenced to the paleohorizontal datum at the time of remanence acquisition. In the case of the Hamblin–Cleopatra Volcano, a previous paleomagnetic study (Ron et al., 1986) proposed significant counter-clockwise rotation (about 29°) for all major fault-bounded blocks in the LMFS. We question whether their sampling density was sufficient as a basis for averaging paleosecular variation within each structural block. We further suggest that the overall in situ and 'corrected' mean determinations were based on too few data to make a statistically significant comparison between observed and expected field directions. In addition, the data were not referenced to a realistic paleohorizontal datum (Geissman et al., 1989). In this study, we have attempted to better document the paleomagnetic record of these rocks and to clarify some of the issues regarding the nature of vertical-axis rotations along the LMFS. Also, our approach in the treatment of in situ data compares different sets of results, corrected in different ways, with expected field directions for samples collected from a volcano with an initial conical morphology.

2. Sampling and laboratory methods

We sampled each of the major lobes and blocks of the structurally dismembered Hamblin–Cleopatra Volcano (Table 1; Fig. 2) along traverses roughly perpendicular to local strike. Orientations of flows, volcaniclastic deposits, and radial dikes were measured (this study; Thompson, 1985), or taken from published maps (Anderson, 1971, 1973; Bohannon, 1979, 1984). Traverses were limited to topographically low areas (e.g. major washes) to avoid influence of lightning strikes. Each traverse is at least 1 km in length and included at least four sites. Each site represents a distinct lava flow, volcaniclastic deposit, dike (and often adjacent host rocks), or sedimentary bed. Each site consisted of 7–18 samples, usually dispersed across the flow or dike. For several dikes, we conducted modified baked contact tests by collecting one or two samples within 2–5 cm of the contact and additional samples at increased distances from the contact. Four traverses were sampled in the Cleopatra Lobe and two in the Hamblin Lobe (Fig. 2).

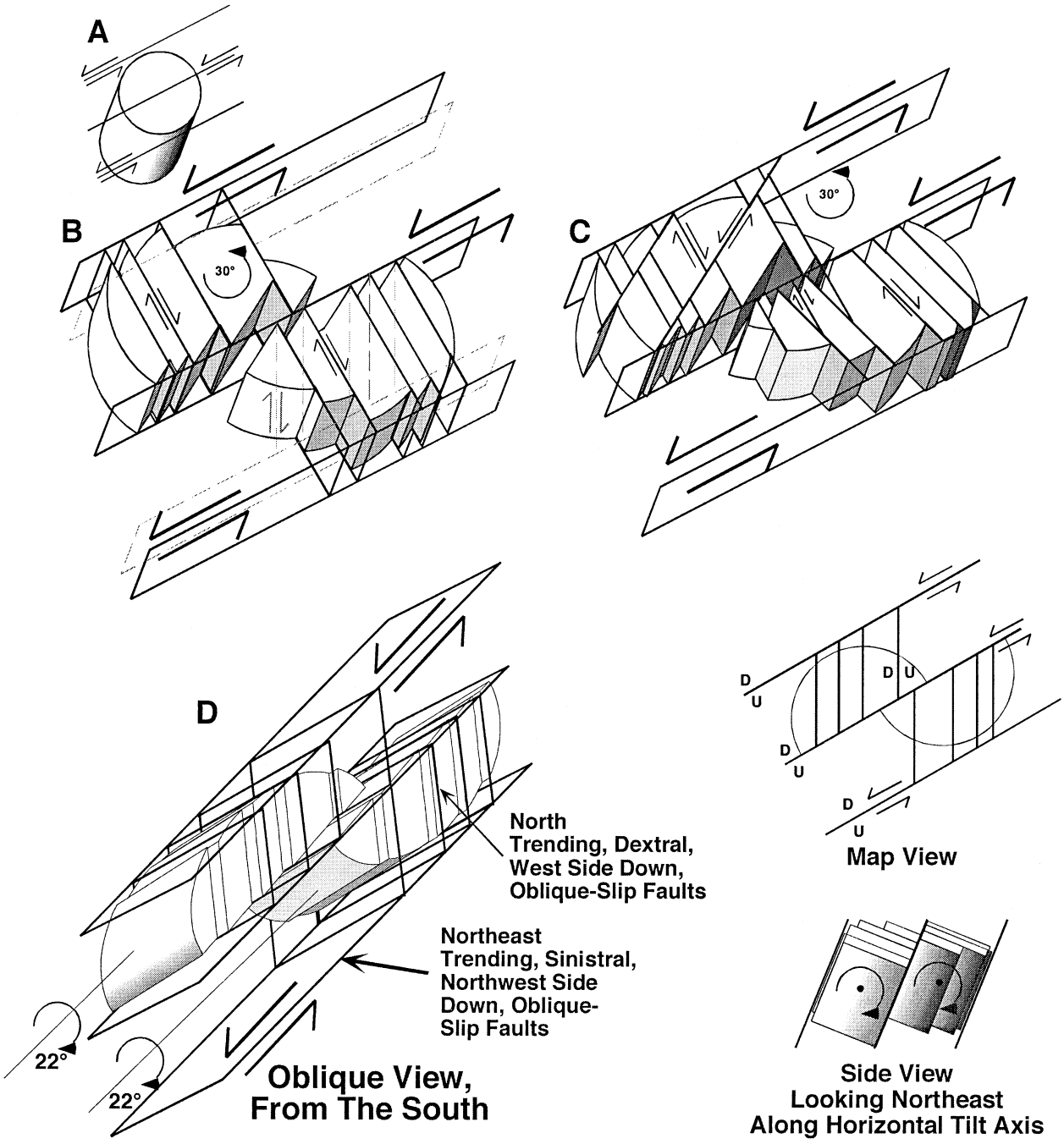

Fig. 4. Possible mechanisms of block rotation within the Lake Mead Fault System in the vicinity of the Hamblin–Cleopatra Volcano. The diagrams are presented in a perspective view, facing north and inclined at a moderate angle. (A) Undeformed, vertical cylinder segmented by an incipient sub-vertical sinistral shear zone. (B) Cylinder is cut by northeast-trending sinistral, strike-slip faults, antithetic dextral shears form with a north-oriented trend to accommodate roughly east–west extension of the crust (consistent with Ron et al. (1986)). The shear-zone widens in a NW–SE direction; the dashed lines show the initial position of all faults. With continued deformation, all faults remain active, and the orientation of faults and fault bounded blocks rotate in a counter-clockwise sense. Note large voids that open along the major sinistral shears. (C) Cylinder is cut by northeast-trending sinistral, strike-slip faults. Northwest half of the cylinder is first cut by north-trending dextral shears that rotate with blocks. At any time, the north-northeast-trending synthetic sinistral shears form and act to conserve volume. If these shears *are kinematically important*, they introduce a *clockwise* vorticity that may impede the *counter-clockwise* rotation produced by the major sinistral faults. The SE half of the cylinder shows an alternative pattern of fault development. As shearing continues, the initial north-trending dextral shears become inactive and new, more favorably oriented dextral shears develop. This process may lead to varying magnitudes of *counter-clockwise*, vertical axis block rotation. It is likely that both of these complex fracture systems are stable in a broad system of anastomosing faults where volume is being conserved. (D) Three views of block deformation associated with oblique shear along all faults. Blocks and faults tilt in a clockwise sense (facing northeast) along horizontal axes parallel to the principal, sinistral, west-side-down, oblique-slip faults. If relatively large amounts of slip occur along the north-trending normal faults, then an additional rotation axis is introduced that is horizontal and parallel to these faults. This possibility is in concert with structural data reported by Anderson (1973) and Thompson (1985) and is consistent with modest amounts of east-side down tilting of parts of the Hamblin–Cleopatra Volcano.

Table 1
Table showing distribution of sites assigned to each traverse with corresponding structural and stratigraphic corrections

Traverse	Sites	Structural correction[a]	Stratigraphic correction[b]
Cleopatra Lobe:			
Cathedral Cove	CC18	170.1°, 21.4°	6°, 27° E
	CC19–CC22	170.1°, 21.4°	344°, 25° E
	CC23	170.1°, 21.4°	327°, 36° E
	CC24–CC25	170.1°, 21.4°	350°, 18° E
	CC26–CC35	170.1°, 21.4°	347°, 30° E
	CC36–CC37	170.1°, 21.4°	333°, 45° E
Cleopatra Cove	HC11–HC27	170.1°, 21.4°	350°, 45° E
	HC50–HC88	170.1°, 21.4°	350°, 45° E
Boat House Cove	HC89–HC96	170.1°, 21.4°	358°, 30° E
Southern Traverse	HC28	170.1°, 21.4°	358°, 25° E
	HC29	170.1°, 21.4°	15°, 20° E
	HC30	170.1°, 21.4°	26°, 20° E
	HC31–HC38	170.1°, 21.4°	18°, 12° E
	HC39	170.1°, 21.4°	13°, 19° E
Central Intrusive:			
Boulder Wash	HC97–HC105	248.7°, 26.6°	278°, 26° N
	HC106–HC114	248.7°, 26.6°	260°, 40° N
Hamblin Lobe:			
Hamblin Mountain	HM1	n/a	186°, 35° W
	HM2–HM7	n/a	109°, 31° S
	HM8–HM10	n/a	117°, 28° S
Sandy Cove	SC1–SC5	n/a	90°, 10° S
	SC6	n/a	307°, 20° E
	SC10–SC17	n/a	307°, 20° E
	SC54–SC60	n/a	0°, 25° E
Hamblin Wash:	HW38–HW53	n/a	n/a
Callville Mesa/West End Wash:	CM1–CM14	n/a	n/a
	CM20–CM32	n/a	n/a
Triassic Red Beds:	HC116–HC119	n/a	5°, 30° E

[a] The structural correction is based on restoring non-vertical dikes in the radial dike swarm, which are sub-parallel to the Hamblin Bay Fault to a hypothetical, vertical orientation; see text.
[b] The stratigraphic corrections are represented as strike and dip of flow contacts sampled over an interval of a traverse. Notation obeys the right hand rule.

Additional localities that are more spatially restricted were sampled to investigate the possibility of small-scale block rotations along the Hamblin Bay Fault or other sinistral structures. These include, from NE to SW, the Boulder Wash traverse, the north end of the Wilson Ridge pluton (Hamblin Bay Wash traverse), and four sites (individual beds) in the Upper Triassic Chinle Formation, directly north of the fault contact between these strata and the intrusive core (Table 2; Fig. 2).

Specimens from at least seven samples per site were stepwise demagnetized in an alternating field (AF) of peak values up to 130 mT. To assess if AF demagnetization isolated all magnetization components contributing to the natural remanent magnetization (NRM), a specimen from at least one sample per site was stepwise thermally demagnetized to peak temperatures of 580°C (for magnetite-dominated rocks) or 680°C (for hematite-dominated rocks). For six sites collected from the Hamblin–Cleopatra Volcano, the principal magnetic phase consisted of hematite, and all samples were thermally demagnetized to peak temperatures of about 680°C. Individual demagnetization results were interpreted using orthogonal demagnetization diagrams of directional data. For 152 of the 192 sites evaluated, demagnetization results indicated the presence of a well-grouped and well-defined magnetization, which in most cases trended to the origin in orthogonal demagnetization diagrams (stable endpoint behavior). This magnetization constituted most of the NRM and could readily be distinguished from a low coercivity, viscous magnetization often roughly parallel to the present day field. In these cases, the directions of magnetizations, isolated over at least three demagnetization steps, were determined using principal components analysis (Kirschvink, 1980) and a site mean direction and associated statistics were determined following the method of Fischer (1953). We also calculated Bingham statistics (Onstott, 1980) to evaluate the possibility of non-circular distributions of sample directions at the site level. Samples from about 20 of the 152 accepted sites exhibited more complex, yet uniform demagnetization behavior, where individual magnetization components

Table 2
Paleomagnetic data of the Hamblin–Cleopatra Volcano (entries in italics are sites that were rejected from mean determinations)

Site number	Rock type	In situ				In situ Bingham statistics			Structural correction		Stratigraphic correction		*C/L*	n/n_T
		D	*I*	α_{95}	κ	α_1	α_2	azm	*I*	*D*	*I*	*D*		
Cathedral Cove Traverse (36.26°N, 114.42°W, 13.5°)														
CC18	Flow	167	−33	7.0	64.7	3.0	7.6	22	181	−32	187	−43	0/7	7/8
CC19	Flow	151	−37	12	46.8	1.4	11.0	65	168	−41	172	−44	0/4	4/8
CC20	Flow	132	−49	10	37.6	1.5	2.2	179	159	−58	165	−62	0/6	6/8
CC21	Flow	137	−58	4.2	257.2	1.3	4.5	147	175	−63	180	−60	0/6	6/8
CC22	Flow	161	−56	7.3	59.5	2.7	7.8	178	192	−53	198	−55	0/8	8/8
CC23	Flow	146	−41	8.5	44.1	4.0	8.4	125	166	−46	178	−40	0/7	7/9
CC24	Flow	154	−47	3.1	279.3	1.4	3.4	97	178	−49	175	−53	0/8	8/8
CC25	Clst	157	−47	3.5	222.6	1.9	3.7	58	181	−47	177	−52	0/8	8/8
CC26	Clst	347	59	7.0	119.5	2.8	7.2	161	30	49	27	48	0/5	5/15
CC27	Flow	317	52	4.8	135.4	3.6	4.6	26	347	59	4.6	64	0/7	7/8
CC28	Clst	345	55	4.1	226.8	1.7	4.2	57	13.9	51	27	52	0/6	6/8
CC29[a]	*Flow*	*171*	*−21*	*9.0*	*46.0*	*3.4*	*8.9*	*113*	*179*	*−19*	*183*	*−23*	*0/6*	*6/8*
CC30	Dike	327	66	10	93.4	3.7	8.9	104	??	??	50	70	0/3	3/9
CC31[a]	*Flow*	*174*	*−15*	*2.7*	*506*	*1.7*	*2.5*	*26*	*179*	*−12*	*183*	*−17*	*0/6*	*6/7*
CC32	Flow	160	−53	5.7	82.5	2.8	6.2	127	188	−51	202	−53	0/8	8/8
CC33	Flow	168	−49	3.1	275.2	1.3	3.5	153	191	−45	202	−47	0/8	8/8
CC34	Flow	166	−56	2.1	634.9	1.1	2.2	114	195	−61	209	−52	0/8	8/8
CC35	Flow	170	−47	7.9	60.1	3.1	8.3	8	191	−43	201	−44	0/7	7/8
CC36	Dike	155	−56	5.6	86.6	2.7	6.1	13	187	−56	208	−41	0/8	8/11
CC37	Flow	356	61	3.5	215.5	1.9	3.7	53	27	53	41	35	0/8	8/8
Cleopatra Cove Traverse (36.2° N, 114.6° W, 13.5°)														
HC11[b]	*Flow*	*144*	*−39*	*24.1*	*12.8*	*15.1*	*23.8*	*31*	*162*	*−45*	*186*	*−43*	*0/5*	*5/8*
HC12	Dike	354	54	5.9	87.5	6.7	18.2	144	19	47	36	33	0/9	9/9
HC13	Dike	344	46	10.6	59.4	9.5	4.3	127	5.5	44	24	34	0/5	5/8
HC14	Clst	311	46	16.7	20.5	17.5	2.5	76	334	56	10	55	0/5	5/8
HC15	Flow	163	−28	5.8	177.6	5.8	1.2	132	174	−28	186	−24	0/5	5/8
HC16	Dike	326	50	7.2	71.9	6.8	4.7	80	353	54	21	47	0/7	7/8
HC17	Flow	142	−49	17.3	27.7	14.8	7.3	107	168	−55	199	−49	0/4	4/8
HC18	Flow	126	−67	7.6	71.0	8.3	10.1	88	186	−73	228	−57	3/4	7/8
HC19	Dike	353	56	3.7	169.2	1.9	4.1	163	20	50	37	34	0/9	9/10
HC20	Flow	1	62	5.2	236.5	3.3	3.6	74	31	52	46	34	0/4	4/8
HC21	Dike	14	52	4.9	246	4.1	3.0	76	32	40	43	22	0/5	5/8
HC22[b]	*Dike*	*106*	*−68*	*61.0*	*2.1*	*24.3*	*8.4*	*54*	*177*	*−80*	*239*	*−63*	*0/6*	*6/8*
HC23	Dike	18.7	61	8.3	98.9	3.0	3.7	123	42	47	52	27	2/3	5/8
HC24[b]	*Clst*	*165*	*−67*	*51.1*	*24.6*	*18.6*	*10.5*	*151*	*207*	*−61*	*228*	*−42*	*0/3*	*3/8*
HC25	Flow	153	−58	12.9	75.3	2.5	1.7	11	188	−58	214	−45	5/0	5/8
HC26	Dike	127	−58	8.7	112.4	7.4	3.4	56	165	−67	211	−59	0/4	4/8
HC27	Dike	139	−55	5.6	274.0	4.1	3.1	144	172	−61	207	−52	0/4	4/8
HC50	Flow	347	46	5.9	88.7	4.0	5.6	31	8	43	25	32	0/7	7/8
HC51	Flow	351	57	8.3	147.4	1.4	6.2	106	20	51	38	36	0/3	3/8
HC52	Dike	347	45	3.5	304.5	1.2	3.7	141	7.3	42	24	32	0/6	6/8
HC53	Flow	156	−54	4.2	694.6	4.1	2.1	304	185	−54	210	−42	5/0	5/8
HC54	Dike	344	52	4.1	163.8	1.9	4.4	108	10	49	30	37	0/8	8/9
HC55[a]	*Dike*	*319*	*−25*	*5.4*	*219.0*	*3.3*	*8.0*	*21*	*312*	*−13*	*310*	*2.3*	*5/1*	*6/8*
HC56	Dike	332	63	12.3	56.8	8.1	10.0	61	14	62	41	47	6/0	7/8
HC57	Dike	350	56	4.3	166.5	1.0	4.9	155	18	51	36	36	0/7	7/8
HC58	Flow	173	−42	6.5	64.5	4.7	6.1	78	191	−38	204	−27	0/8	8/8
HC59	Flow	351	51	6.9	101.3	4.0	6.8	160	16	46	32	33	6/1	7/8
HC60	Dike	359	64	3.2	306.1	2.1	3.1	53	32	55	47	36	0/7	7/8
HC61	Flow	150	−51	2.7	312.6	2.2	2.5	24	178	−53	204	−45	0/9	9/9
HC62	Flow	138	−34	3.4	306.5	3.8	15.9	131	154	−43	177	−45	0/7	7/8
HC63	Flow	347	52	4.8	290.8	3.2	4.1	168	12	49	31	36	2/3	5/8
HC64	Flow	176	−55	4.3	213.7	2.4	6.1	154	202	−48	217	−33	7/1	8/8
HC65	Flow	177	−54	9.5	94.9	8.7	15.2	175	202	−47	217	−31	0/4	4/8
HC66	Flow	209	−69	11.0	30.5	7.9	13.0	122	231	−49	239	−27	3/5	8/8
HC67	Dike	337	49	2.2	651.0	1.4	2.1	141	2	49	23.9	39	0/7	7/8
HC68	Clst	103	−71	7.3	86.0	7.7	15.3	161	197	−82	244	−62	0/6	6/8
HC69	Flow	174	−63	4.3	346.8	0.8	3.9	127	208	−55	225	−37	0/4	4/8

Table 2 (*continued*)

Site number	Rock type	In situ				In situ Bingham statistics			Structural correction		Stratigraphic correction		*C/L*	n/n_T
		D	*I*	α_{95}	κ	α_1	α_2	azm	*I*	*D*	*I*	*D*		
HC70[a]	*Dike*	*14.0*	*−73*	*7.9*	*202.4*	*1.6*	*18.7*	*173*	*308*	*−69*	*284*	*−50*	*5/0*	*5/8*
HC71[a]	*Dike*	*252*	*−78*	*6.3*	*113.3*	*4.2*	*5.6*	*149*	*257*	*−57*	*258*	*−33*	*0/6*	*6/8*
HC72	Flow	141	−58	2.2	721.6	1.8	1.8	88	179	−62	212	−51	0/7	7/9
HC73	Dike	342	55	10.7	75.8	9.7	12.9	154	12	52	33	39	0/4	4/8
HC74[b]	Flow	165	−27	15.2	15.6	12.1	20.2	161	176	−27	186	−22	8/1	9/9
HC75	Dike	182	−59	11.2	42.1	4.6	22.5	119	209	−49	223	−32	7/0	7/8
HC76[b]	Flow	8.9	60	9.2	57.1	7.2	9.7	156	35	48	47	30	6/1	7/8
HC77	Flow	144	−39	4.3	199.8	4.7	14.8	161	163	−45	186	−43	0/7	7/8
HC78	Dike	164	−45	8.7	48.3	9.5	16.0	20	185	−43	202	−33	0/7	7/8
HC79	Dike	169	−49	3.9	291.4	3.7	5.1	129	192	−45	209	−33	0/6	6/8
HC80[b]	Clst	100	27	75.1	1.3	27.2	41.5	106	98	6.7	98	−16	0/12	12/12
HC81	Flow	332	59	15.8	35.1	10.5	14.5	149	9	59	35	46	0/4	4/8
HC82	Flow	165	−34	11.9	31.4	12.4	20.0	45	179	−33	193	−26	0/6	6/8
HC83	Flow	151	−64	6.2	93.3	3.6	6.2	20	195	−63	222	−47	0/7	7/8
HC84	Flow	114	−66	8.2	55.0	8.7	25.7	167	175	−77	231	−62	0/7	7/7
HC85	Flow	166	−68	3.8	215.5	3.8	2.2	134	210	−61	230	−42	0/7	7/7
HC86	Flow	119	−51	6.0	102.8	3.7	5.8	155	146	−65	197	−64	0/7	7/8
HC87	Dike	208	−52	4.5	375.5	2.5	8.5	38	223	−36	229	−17	6/0	6/8
HC88	Dike	321	53	5.3	112.1	3.0	5.3	91	353	59	24.9	50	0/7	7/8
Southern Traverse of the Cleopatra Lobe (36.2° N, −114.6° W, 13.5°)														
HC28	Dike	164	−12	4.5	154.2	2.6	5.5	163	171	−13	172	−16	9/0	9/12
HC29	Clst	8	60	7.2	74.8	5.5	8.9	163	34	48	41	56	5/2	6/8
HC30	Sill	172	−20	4.3	238.3	0.3	3.8	355	180	−18	0	31	3/0	3/8
HC31	Mud	4	51	3.8	257.2	1.8	3.8	32	25	42	19	52	0/6	6/7
HC32	Dike	166	−60	8.1	114.1	7.8	2.8	54	199	−55	187	−64	0/5	5/8
HC33	Dike	174	−26	12.8	77.4	6.9	9.5	6	184	−23	180	−30	5/0	5/8
HC34	Flow	169	−50	3.6	352.8	3.7	1.1	34	193	−46	183	−55	0/6	6/8
HC35	Flow	157	−46	17.1	37.7	10.9	7.0	129	180	−47	168	−53	0/5	5/8
HC36[b]	*Dike*	*202*	*71*	*6.3*	*191.0*	*2.6*	*22.3*	*105*	*136*	*71*	*169*	*68*	*6/0*	*6/8*
HC37[b]	*Flow*	*197*	*61*	*6.4*	*90.6*	*7.1*	*1.7*	*20*	*155*	*63*	*177*	*59*	*0/6*	*6/8*
HC38[b]	*Flow*	*181*	*20*	*7.2*	*86.8*	*6.8*	*4.0*	*35*	*173*	*23*	*177*	*16*	*0/6*	*6/8*
HC39	Flow	145	−69	6.5	87.2	6.9	2.7	41	202	−68	205	−76	0/7	7/8
Boat House Cove Traverse of the Cleopatra Lobe (continued)														
HC89	Flow	336	59	5.1	111.2	4.2	5.2	88	11	57	27	57	4/5	9/11
HC90	Flow	338	41	9.5	54.3	5.7	12.1	83	357	42	6	44	6/1	7/10
HC91	Flow	251	38	6.3	104.8	4.1	4.9	147	246	59	234	65	6/8	6/8
HC92	Flow	259	30	7.5	64.8	3.2	8.1	47	258	51	253	59	4/3	7/8
HC93	Flow	172	−37	5.2	136.4	1.4	5.8	61	187	−33	194	−34	6/1	7/8
HC94	Flow	301	26	9.9	46.9	3.0	10.4	33	311	41	316	49	6/0	6/8
HC95	Flow	301	45	4.5	224.1	1.5	4.7	142	323	59	335	65	6/0	6/8
HC96	Flow	310	53	14.0	19.4	2.3	15.4	121	341	62	360	66	5/2	7/8
Boulder Wash Traverse (Central Intrusive core: 36.19° N, −114.6° W, 13.5°)														
HC97	Dike	144	−57	10.3	90.2	6.0	8.9	2	–	–	–	–	4/1	5/10
HC98	Dike	359	60	5.5	125.2	1.5	5.9	128	–	–	–	–	5/1	6/8
HC99	Flow	192	−46	8.4	178.3	3.9	11.5	173	–	–	–	–	5/0	5/8
HC100[a]	*Flow*	*287*	*48*	*13.8*	*26.2*	*6.2*	*15.8*	*118*	–	–	–	–	*1/6*	*7/9*
HC101	Flow	5	67	9.4	46.3	3.8	4.5	168	–	–	–	–	3/4	7/8
HC102	Dike	3	61	7.1	75.3	3.5	7.0	100	–	–	–	–	0/6	6/8
HC103	Flow	114	−30	11.7	36.7	8.4	12.1	142	–	–	–	–	3/3	6/9
HC104	Dike	185	−54	7.8	204.0	3.2	9.5	50	–	–	–	–	5/0	5/8
HC105	Cong	11	52	13.2	22.2	7.3	3.6	8.3	–	–	–	–	1/6	7/8
HC106	Cong	8	56	4.2	265.2	1.8	4.0	156	–	–	–	–	0/5	5/8
HC107	Flow	207	−66	4.1	528.4	1.8	11.8	124	–	–	–	–	5/0	5/10
HC108[a]	*Flow*	*112*	*7*	*7.4*	*71.6*	*3.1*	*9.2*	*31*	–	–	–	–	*7/1*	*8/8*
HC109[a]	*Dike*	*104*	*−11*	*9.4*	*49.3*	*1.0*	*28.3*	*141*	–	–	–	–	*3/0*	*3/8*
HC110	Dike	125	−8.5	4.4	473.5	2.4	5.3	151	–	–	–	–	4/1	5/8
HC111[a]	*Flow*	*117*	*14*	*6.4*	*95.2*	*4.5*	*13.5*	*36*	–	–	–	–	*7/1*	*8/8*
HC112	Skrn	155	−52	14.4	60.7	6.2	15.9	127	–	–	–	–	5/0	5/8
HC113	Dike	28	63	10.1	38.5	4.9	5.8	116	–	–	–	–	2/5	7/8
HC114	Dike	140	−12	7.6	76.1	5.4	10.4	152	–	–	–	–	5/2	7/9

Table 2 (*continued*)

Site number	Rock type	In situ				In situ Bingham statistics			Structural correction		Stratigraphic correction		*C/L*	n/n_T
		D	*I*	α_{95}	κ	α_1	α_2	azm	*I*	*D*	*I*	*D*		
Hamblin Mountain Traverse (36.13°N, −114.6° W, 13.5°)														
HM1	Flow	179	−66	3.3	408.1	2.6	2.6	116	–	–	132	46	0/6	6/8
HM2	Flow	200	74	4.7	202.0	3.7	3.7	139	–	–	199	43	0/6	6/7
HM3	Flow	231	74	3.4	386.6	2.7	2.7	165	–	–	211	45	0/6	6/7
HM4	Flow	234	79	4.2	256.9	3.3	3.3	163	–	–	209	49	0/6	6/7
HM5	Flow	217	68	6.5	107.3	5.1	5.1	72	–	–	207	38	0/6	6/7
HM6	Flow	215	68	5.2	138.5	4.2	4.2	8.5	–	–	206	38	0/7	7/8
HM7[a]	*Flow*	*111*	*13*	*121*	*1.3*	*49.5*	*107.1*	*83.8*	–	–	*121*	*15*	*0/4*	*4/10*
HM8	Flow	260	49	20.6	23.2	13.5	15.9	128	–	–	246	33	1/3	4/7
HM9	Flow	239	36	15.6	17.1	11.1	17.1	163	–	–	234	16	3/4	7/8
HM10	Flow	48	59	5.2	169.2	4.0	4.0	35	–	–	110	79	0/6	6/7
Sandy Cove Traverse of the Hamblin Lobe (36.15° N, −114.66° W, 13.5°)														
SC1	Flow	135	−44	6.9	57.6	5.7	5.8	126	–	–	126	−51	0/8	8/8
SC2	Flow	161	−60	4.7	121.4	4.0	4.0	36	–	–	153	−69	0/10	10/11
SC3	Flow	175	−57	5.3	97.5	4.4	4.4	173	–	–	173	−67	0/8	8/8
SC4	Flow	166	−61	5.1	103.4	4.6	4.6	161	–	–	160	−70	0/7	7/8
SC5	Flow	162	−60	5.2	174.9	3.8	3.8	13	–	–	154	−69	0/5	5/8
SC6	Flow	180	−73	3.8	321.2	3.6	3.6	7.2	–	–	201	−57	0/6	6/8
SC10	Clst	166	−77	3.7	228.3	3.0	3.0	162	–	–	196	−60	0/7	7/8
SC12	Dike	182	−35	8.1	57.7	6.3	6.4	176	–	–	187	−18	0/6	6/8
SC13[a]	*Flow*	*281*	*−3.9*	*11.3*	*22.1*	*16.9*	*18.9*	*9*	–	–	*281*	*5*	*0/8*	*8/8*
SC14[a]	*Flow*	*297*	*−6.0*	*3.2*	*259.0*	*2.7*	*2.7*	*39*	–	–	*296*	*−2*	*0/8*	*8/8*
SC15	Flow	161	−45	16.3	24.6	10.3	10.6	60	–	–	173	−32	0/4	4/8
SC16	Flow	187	−52	5.2	372.3	2.8	2.8	76	–	–	195	−34	0/3	3/8
SC17	Flow	177	−52	5.6	121.1	4.4	4.4	173	–	–	188	−35	0/6	6/9
SC54	Flow	160	−64	4.2	179.4	3.4	3.4	179	–	–	211	−61	0/7	7/8
SC55	Flow	144	−65	5	95.3	4.3	4.3	37	–	–	205	−68	0/9	9/9
SC56	Flow	148	−73	6.4	75.8	5.2	5.3	127	–	–	227	−69	0/7	7/8
SC57	Flow	153	−57	10.5	35.5	8.2	8.4	59	–	–	195	−60	0/6	6/8
SC58	Flow	181	−36	7.8	167.4	4.2	4.2	92	–	–	198	−32	0/3	3/8
SC59	Flow	193	−48	4.1	142.7	3.5	3.5	39	–	–	215	−38	0/9	9/12
SC60[c]	*Clst*	–	–	–	–	–	–	–	–	–	–	–	–	–
SC61	Flow	175	−59	3.7	153.9	2.3	3.9	4	–	–	212	−53	0/11	11/11

[a] Rejected because site mean was greater than $2\theta_{63}$ from traverse or block mean.
[b] Site rejected because of excessively high value of α_{95}.
[c] Site consisted of an autoclastic breccia that was use for a conglomerate test (see Fig. 7).

appear to overlap in coercivity or laboratory unblocking temperature. To resolve the last-removed magnetization at the site level, a combination of stable endpoint and great circle analysis (Method 2 of Kirschvink, 1980) was applied to estimate site mean directions and Bingham statistics were applied. To determine if any of these directions are representative of a time-averaged geomagnetic field, we applied the reversal test of McFadden and McElhinny (1990). We grouped the data for this analysis at both the traverse and block levels and achieved varied results (Table 4). Of all the traverse sample collections, only the Cleopatra Wash and Southern traverses yielded normal and reverse polarity mean directions that appear to be 180° apart (actual angular difference is less than the critical angle cutoff whose value is dictated by the statistical variation of the normal and reverse polarity data sets). When the traverses were combined into groups based on individual fault blocks, the samples from the Cleopatra Lobe and the central core also pass the reversal test. The absence of any bi-polarity data derived from samples collected in the Hamblin Lobe precluded the application of this analysis.

The definition of a realistic structural correction to restore site mean directions from in situ, geographic coordinates to a pre-extension, pre-faulting orientation is critical. For most paleomagnetic investigations, a structural or 'bedding' correction is based on field measurements of tilted strata and data are restored about the present strike axis. However, deposits from andesitic composite volcanoes typically dip radially outward from the central cone. Proximal dip values can be considerable and highly variable. For example, a mean radial dip based on morphometric measurements from 200 andesitic composite volcanoes is $24 \pm 9°$ (1σ) (Pike and Clow, 1981; Cas and Wright, 1987). Although the lateral extent of lavas and associated deposits and overall geometry of the Hamblin–Cleopatra Volcano prior to deformation are not known, we assume that overall morphology of the volcano was probably that of a typical, somewhat circularly symmetric strato-volcano. In principle,

an accurate restoration of paleomagnetic data from deposits of the volcano to a 'paleohorizontal' datum should also restore present-day observed flow orientations to a realistic approximation of a conical morphology for the volcano. Our approach to evaluating the paleomagnetic data therefore considers three types of directions: (1) in situ site mean and traverse means, (2) values based on restoring observed flow orientations to an idealized conical form for the volcano, and (3) values based on stratigraphic corrections, where layered rocks are fully untilted about the present strike axes. Where applicable, the stratigraphic tilt measurements are averaged into a single correction for each traverse (Table 1), as each traverse is oriented in a radial fashion with respect to the core of the volcano. The determination of a partial structural correction for a specific block involves the assumption that dikes comprising the radial swarm and the lavas of the volcano are essentially coeval and that these dikes were vertical prior to strike-slip faulting and any attendant local tilting. The dike corrections, given the manner in which they were determined, are applied to entire blocks. The validity of these assumptions can be addressed by application of the 'volcano-test', as described by Ron et al. (1986). A 'positive' result is obtained if the dispersion of the data, as measured by a decrease in Fisher's (1953) estimate of the precision parameter, k, increases as the flows are restored, using stratigraphic tilt corrections, to an unrealistic horizontal plane. For each traverse, the different paleomagnetic determinations were compared with expected middle- to late-Miocene field directions (Irving and Irving, 1982; Mankinen et al., 1987; Calderone et al., 1990).

3. Results

Examples of orthogonal demagnetization diagrams reveal that, overall, the response of rocks of the Hamblin Cleopatra Volcano to progressive demagnetization was straightforward (Figs. 5–7). NRM intensities of rocks without hematitic pigmentation (visibly unoxidized) range from about 0.2 to 0.8 A/m; rocks with hematitic pigmentation had NRM intensities ranging from 0.001 to 2.0 A/m. In general, samples treated by progressive alternating field or thermal demagnetization displayed stable-end-point behavior characterized by the removal of any apparent secondary magnetization by 5–20 mT or between 150 and 500°C, respectively. For some samples requiring AF treatment above 100 mT, the acquisition of an anhysteretic remanent magnetization complicated interpretation of demagnetization results. This behavior, however, was not consistent over any given site and, therefore, had little bearing on the site mean direction determined from such sites. Limited field-based magnetization tests (i.e. baked contact and conglomerate tests) verify or support the antiquity of the resolved magnetizations, although in this particular setting, there is little reason to suspect that the rocks have been pervasively remagnetized by some, or a combination of, processes since middle- to late-Miocene magmatism. Overall, the observed demagnetization behavior varied through each traverse, with the finest-grained, most mafic materials having relatively high median destructive fields and high, relatively narrow laboratory unblocking temperatures below about 580°C. Coarser, more intermediate composition rocks typically had lower median destructive fields and more distributed laboratory unblocking temperatures.

3.1. Traverses of the Cleopatra Lobe

From north to south, the traverses within the Cleopatra Lobe include the Cathedral Cove, the Cleopatra Cove, the Southern traverse and the Boathouse Cove traverse (Table 1; Fig. 2). Although the Boathouse Cove traverse is located within a structural block that is separate and distinct from the Cleopatra Lobe, the paleomagnetic results are statistically indistinguishable from all other data from the lobe proper. Each traverse yielded site means of both normal and reverse polarity. At the site level, generally, no more than two magnetizations were isolated in progressive demagnetization. Relatively high-coercivity or high laboratory unblocking temperature magnetizations are well-grouped at the site level and are typically well-defined by stable end-point behavior over much of the range of demagnetization treatments. For most sites, a thermally demagnetized sample from each site yielded demagnetization behavior similar to that during AF demagnetization. The exceptions were defined on the basis of negligible response to AF demagnetization. In this case, the principal magnetic phase was either hematite or very high coercivity magnetite, in which case complete unblocking of magnetizations was reached at temperatures below 580°C. Where hematite appeared to be the principal magnetic phase, thermal demagnetization resulted in stable end-point decay over a laboratory unblocking temperature range between 600 and 680°C.

Samples from the 19 accepted sites along the Cathedral Cove traverse responded well to AF demagnetization and yielded well-defined site mean directions; the only rejected site was CC26, which is a matrix-supported polylithologic volcanic breccia. The matrix is a gray, medium grained, poorly sorted lithic arenite. In AF demagnetization to 135 mT, all the samples from the matrix maintained at least 60% of their NRM intensities. Thermal demagnetization treatment up to 580°C resulted in complete unblocking of the remanent magnetization. Demagnetization diagrams revealed stable end-point behavior and unblocking was consistent in all five matrix samples (Table 2; Fig. 5b). The clasts demagnetized well using AF treatment and, between clasts, the magnetizations isolated are random at a 95% confidence level (Watson, 1956), implying that the magnetizations in the clasts have not been modified since incorporation in the deposit. Two dikes were sampled along the Cathedral Cove traverse (sites CC30 and CC36). Although no contact tests were conducted in relation to

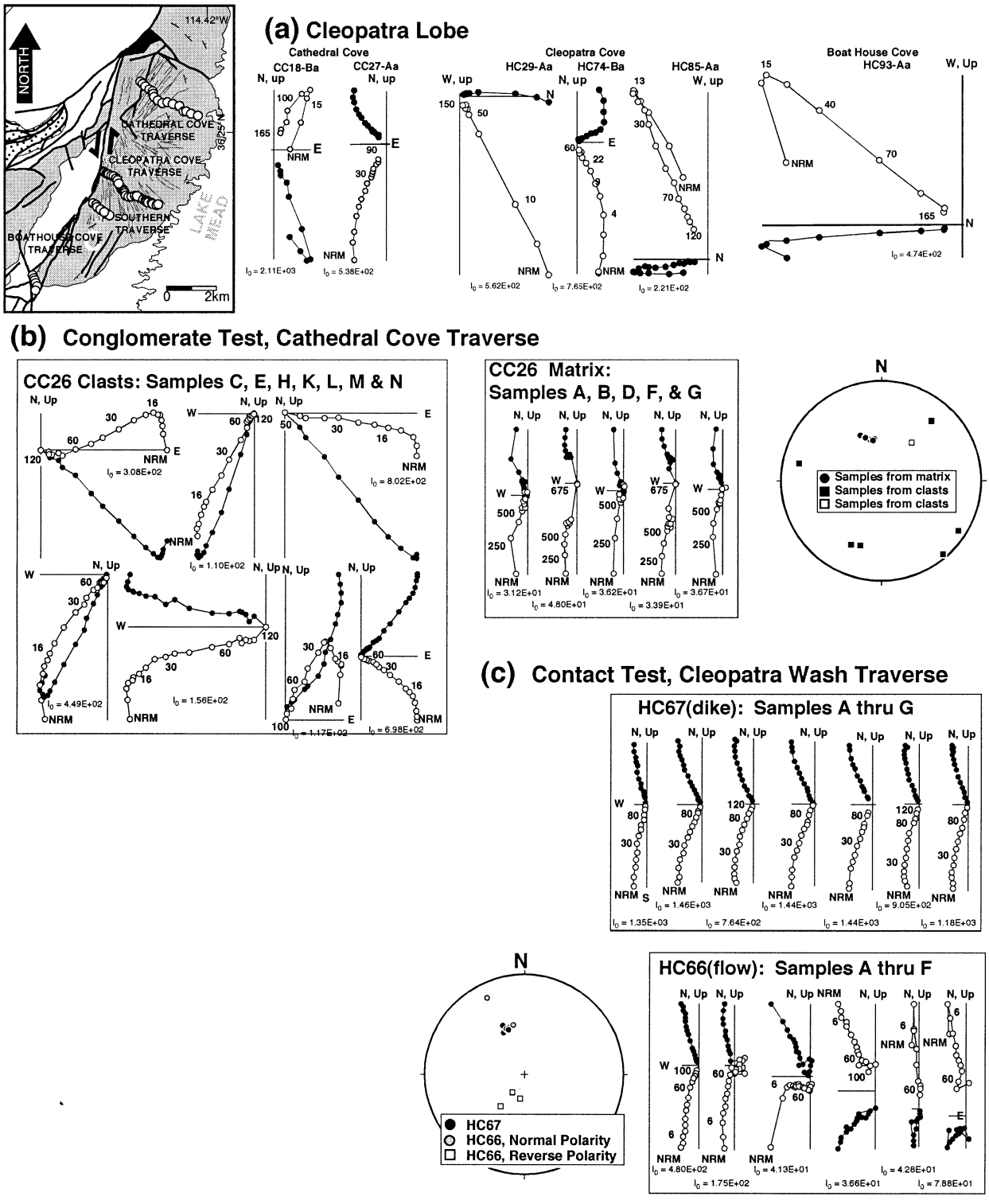

Fig. 5. Paleomagnetic results from the Cleopatra Lobe. Inset map (from Fig. 2) shows the location of the traverses in the Cleopatra Lobe. (a) Representative orthogonal demagnetization diagrams (Zijderveld, 1967) from traverses within the Cleopatra Lobe. (b) Equal-area, lower-hemisphere projection and associated demagnetization diagrams of results from a successful conglomerate test for site CC26, Cathedral Cove traverse. The matrix consists of fine-grained, red colored (hematitic) sandstone. (c) Equal area, lower-hemisphere projection and orthogonal demagnetization diagrams of all samples from a contact test conducted between sites HC67 (intermediate composition dike) and HC66 of the Cleopatra Wash traverse. NRM intensities (I_0) for specimens in all demagnetization diagrams are given in mA/m.

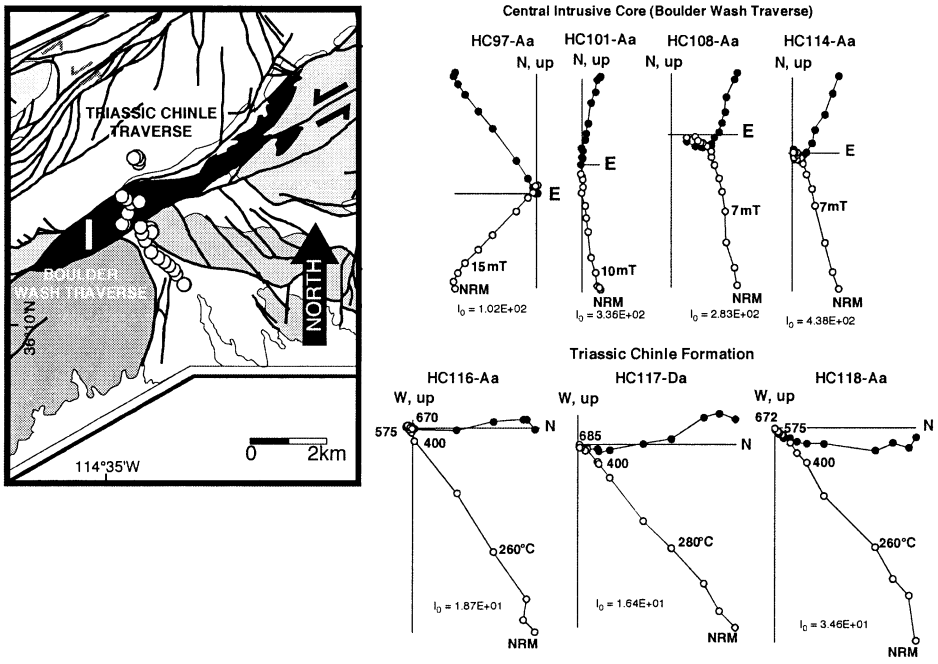

Fig. 6. Paleomagnetic results for the central intrusive core and nearby Triassic Chinle Formation. Inset map (taken from Fig. 2) shows the location of the traverses in the central part of the Hamblin–Cleopatra Volcano along the Lake Mead Fault System, which exposes the central intrusive core and nearby, fault contacted, Mesozoic sedimentary rocks. Representative orthogonal demagnetization diagrams from volcanic rocks (demagnetization steps are in mT) sampled in the Boulder Wash traverse and from Triassic Chinle strata are also shown (demagnetization steps are in °C). NRM intensities (I_0) for specimens in all demagnetization diagrams are given in mA/m.

these two sites, the results from CC30 were more complex than those from CC36. Three samples from the dike interior yielded a well grouped, normal polarity mean direction (Table 2). The remaining six samples from the dike margins displayed stable-end point behavior yet yielded magnetizations that were random at a 95% confidence level and were rejected from the site mean. Such extreme dispersion is not typical of efficiently remagnetized rocks, nor is it characteristic of a single, relatively rapidly cooled intrusion with an efficient TRM. Finally, the reversal test (McFadden and McElhinny, 1990) along this specific traverse failed (normal polarity sites: mean $D/I = 347°/55°$; reverse polarity sites: mean $D/I = 159°/-45°$; $k_n/k_r = 2.1$, critical angle = 11.6°; actual angle = 15.3°).

The Cleopatra Wash traverse is the most extensive of the four traverses in both breadth of coverage of the volcanic sequence and in number of sites. Only four of the 56 sites required thermal demagnetization to fully isolate all components of the NRM. During demagnetization, samples from these sites unblocked between about 500 and 580°C. Tests of the antiquity of the magnetization included a reversal test, conglomerate tests (sites HC24 and HC80) and many baked contact tests that were completed as part of sampling some of the 24 dikes along this traverse. Volcanic agglomerate clasts sampled at sites HC24 and HC80 yielded randomly directed magnetizations with no two clasts yielding a common direction. The results obtained from these two sites constitute positive conglomerate tests. In all but two of the baked contact tests, either no thermal effects were noticeable within host rock samples or the magnetizations of the dike and host rock were too similar in direction to convincingly evaluate effects of dike intrusion, yielding inconclusive baked contact tests. Data from the dike sampled at HC67 (normal polarity) and the associated host rock at site HC66 (reverse polarity) provide an example of a positive baked contact test (Fig. 5c). At site HC66, samples in the lava flow contain an overprint of normal polarity that is similar to the direction isolated in the dike at site HC67. The relative intensity of the overprint increases in samples collected closest to the dike contact. Two samples collected within 4–6 cm of the contact are completely remagnetized, with a direction statistically indistinguishable from the mean direction determined for site HC67. In total, the sites from this traverse passed the reversal test (Table 4, Class B).

The southern traverse is located within an unnamed cove about 1.5 km south of Cleopatra Cove (Figs. 2 and 5a). All 12 sites from this traverse yielded well-defined results, but only seven site means, which passed a reversal test (Table 4), were used in the final determination of the in situ mean direction for the Cleopatra Lobe (Table 5). The rocks sampled included four dikes, one sill, an agglomerate flow, one autoclastic breccia with a fine-grained matrix, and five lava flows. Three sites (HC36–HC38) were rejected because the resolved magnetizations were of south-directed declination yet of moderate positive inclination (Table 2); these sites probably sampled a transitional field. Similarly,

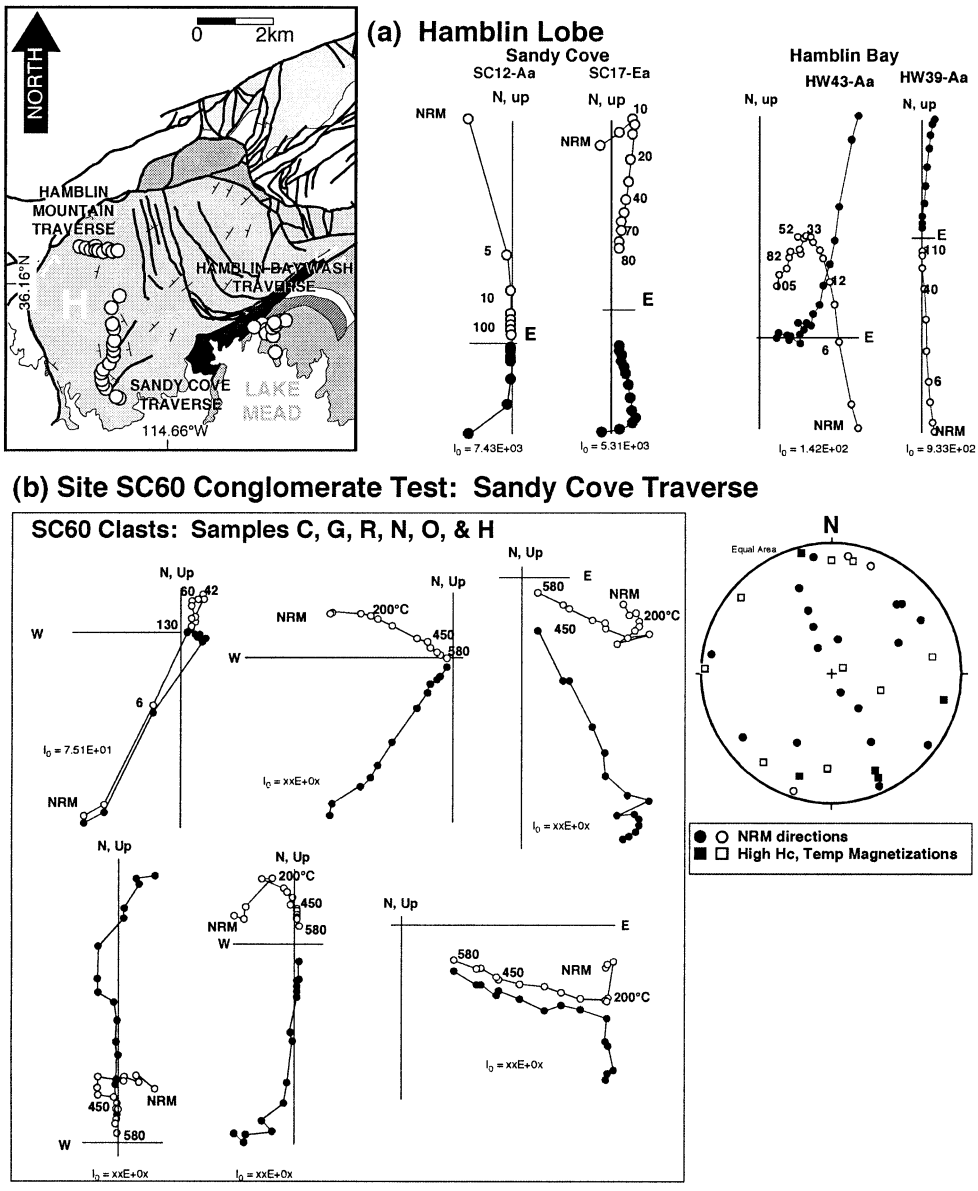

Fig. 7. Paleomagnetic results from the western end of the Hamblin–Cleopatra Volcano. Inset map (from Fig. 2) shows the location of the traverses in the Hamblin Lobe and the dike complex (northernmost part of the Wilson Ridge Complex) south of the Hamblin Bay Fault (see text). (a) Representative orthogonal demagnetization diagrams from the Hamblin Lobe and nearby dike complex. (b) Equal-area, lower-hemisphere projection and associated demagnetization diagrams of results from a successful conglomerate test conducted along the Sandy Cove traverse. At this site, the matrix consists of poorly sorted, coarse-grained, light gray to gray–green sandstone that did not yield interpretable demagnetization results. NRM intensities (I_0) for specimens in all demagnetization diagrams are given in mA/m. The missing NRM intensities for specimens SC60 G, R, N, O, and H are 3.01E + 02, 2.31E + 03, 8.34 + 02, 9.43E + 02, and 2.00E + 03, respectively.

two sites (HC28 and HC30) yielded south declination and very shallow negative inclination magnetizations, and were also rejected on similar grounds. Of the remaining sites, stable end-point behavior characterized demagnetization behavior. Five sites had high-coercivity, secondary magnetizations that were not fully removed during progressive alternating field demagnetization. Assuming the presence of only two magnetizations in any one sample associated with these sites, principal component analysis resolved a magnetization with a direction consistent with the principal magnetization isolated by thermal demagnetization on duplicate specimens. Seven limited-scope, baked-contact tests were completed and two yielded conclusive results that show that the magnetizations were acquired during initial cooling of the rocks. For example, data from the sill sampled at HC30 appear to be consistent with remagnetization of a sample from site HC29, in an overlying agglomerate, collected within 2 cm of the intrusive contact. No thermal effects were noted, however, in the underlying breccia deposit at site HC31. The dike/dike contact involving sites HC32 and HC33 also provided a positive contact test. The dike at site HC32 yielded a well-grouped reverse

Table 3
Paleomagnetic data in the vicinity of the Hamblin–Cleopatra Volcano

Site number	Rock type	In situ				In situ Bingham statistics			Structural correction		Stratigraphic correction		*C*/*L*	n/n_T
		D	*I*	α_{95}	κ	α_1	α_2	azm	*I*	*D*	*I*	*D*		
Hamblin Wash Traverse (Wilson Ridge pluton: 36.15° N, −114.63° W, 13.5°)														
HW38	Dike	10	63	7.5	105.1	3.4	6.9	17	–	–	–	–	5/0	5/8
HW39	Dike	2	58	3.1	501.6	1.5	2.8	58	–	–	–	–	0/5	5/8
HW40	Dike	152	−66	5.5	182.5	2.5	12.4	58	–	–	–	–	7/0	7/8
HW41	Dike	113	−67	7.9	137.5	4.0	6.2	10	–	–	–	–	0/4	4/8
HW42[a]	*Dike*	–	–	–	–	–	–	–	–	–	–	–		
HW43	Dike	164	−66	11.8	223.1	1.7	8.7	164	–	–	–	–	4/0	4/5
HW44	Dike	67	−79	6.7	168.3	3.7	16.1	155	–	–	–	–	6/0	6/8
HW45[b]	*Dike*	*64*	*−29*	*14.4*	*49.8*	*0.8*	*10.9*	*52*	–	–	–	–	*0/3*	*3/8*
HW46	Dike	104	−54	4.0	195.5	1.5	4.4	87	–	–	–	–	0/7	7/9
HW47	Dike	100	−52	9.9	38.7	2.6	11.2	81	–	–	–	–	6/0	6/8
HW48[a]	*Dike*	–	–	–	–	–	–	–	–	–	–	–	–	–
HW49	Dike	114	−78	13.7	164.1	4.1	12.5	110	–	–	–	–	4/8	4/8
HW50	Dike	182	−29	4.4	192.0	0.9	4.7	171	–	–	–	–	8/12	8/12
HW51	Dike	14	67	13.4	29.6	9.3	12.1	163	–	–	–	–	5/1	6/9
HW52	Dike	175	−34	6.5	91.7	4.9	9.5	176	–	–	–	–	7/1	8/10
HW53	Dike	176	−53	13.2	32.4	7.5	12.3	47	–	–	–	–	8/0	8/10
Triassic Chinle Formation Traverse (36.2° N, −114.57° W, 13.5°)														
HC116	Silt	39	30	5.1	224	3.8	3.8	82	–	–	301	17	0/5	5/5
HC117	Silt	32	36	21.4	15.6	14.3	18.4	29	–	–	49	25	2/3	5/5
HC118	Silt	41	39	13.1	53.5	7.1	14.8	43	–	–	57	23	4/1	5/5
HC119	Silt	30	38	8.3	124	5.5	5.5	157	–	–	49	27	0/4	4/4
Callville Mesa and West End Wash Basalts) (36.15° N, −114.75° W, 13.5°)														
CM1	Flow	25	33	5.7	72.6	4.7	5.2	32	–	–	–	–	0/9	9/10
CM2	Flow	27	41	3.1	399.1	1.7	2.9	32	–	–	–	–	0/6	6/8
CM3	Flow	36	47	3.5	218.2	2.3	3.4	20	–	–	–	–	0/8	8/8
CM4	Flow	39	42	5.1	178.8	2.6	4.7	28	–	–	–	–	0/5	5/8
CM5	Flow	24	51	3.4	554.0	1.6	2.2	81	–	–	–	–	0/7	7/8
CM6	Flow	36	16	6.4	79.7	5.3	7.5	50	–	–	–	–	0/8	8/8
CM7	Flow	41	23	4.6	211.9	1.8	4.8	6.8	–	–	–	–	0/6	6/8
CM8	Flow	36	18	2.9	421.6	0.7	3.3	129	–	–	–	–	0/7	7/8
CM9	Flow	44	38	6.3	94.8	2.8	6.4	120	–	–	–	–	0/6	6/8
CM10	Flow	33	35	4.9	130.9	1.3	5.5	141	–	–	–	–	0/7	7/7
CM11	Flow	38	32	3.5	304.2	2.5	3.0	111	–	–	–	–	0/6	6/8
CM12	Flow	38	29	6.1	128.4	2.6	5.8	6	–	–	–	–	0/5	5/8
CM13	Flow	40	39	5.8	111.4	3.4	5.5	82	–	–	–	–	0/6	6/8
CM14	Flow	43	36	5.3	135.5	2.2	5.4	19.8	–	–	–	–	0/6	6/8
WE20	Flow	29	46	4.6	178.3	1.4	4.9	32	–	–	–	–	0/6	6/8
WE21	Flow	12	47	4.0	166.0	2.9	3.8	79	–	–	–	–	0/8	8/8
WE22	Flow	13	41	3.2	306.5	1.8	3.2	168	–	–	–	–	0/7	7/8
WE23	Flow	17	49	3.7	192.7	1.9	4.0	81	–	–	–	–	0/8	8/9
WE24	Flow	32	52	5.0	94.2	2.9	5.4	47	–	–	–	–	0/9	9/9
WE25	Flow	23	54	3.3	245.2	2.2	3.2	166	–	–	–	–	0/8	8/8
WE26	Flow	9	59	3.0	297.6	1.0	3.4	45	–	–	–	–	0/8	8/9
WE27	Flow	24	58	5.2	98.5	1.6	6.0	165	–	–	–	–	0/8	8/8
WE28	Flow	38	56	2.3	443.8	1.5	2.4	6	–	–	–	–	0/9	9/9
WE29	Flow	37	54	4.4	160.1	2.9	4.2	25	–	–	–	–	0/7	7/8
WE30	Flow	47	54	4.4	166.1	2.3	4.5	148	–	–	–	–	0/7	7/8
WE31	Flow	44	60	2.3	433.6	0.9	2.7	133	–	–	–	–	0/9	9/9
WE32	Flow	37	62	2.0	774.2	1.2	2.0	16	–	–	–	–	0/7	7/8

[a] During laboratory analysis, samples from these sites behaved as a diamagnetic or paramagnetic material.
[b] Rejected because site mean was greater than $2\theta_{63}$ from traverse or block mean.

polarity site mean. Host rocks at HC33 were variably affected, with the three samples closest to the dike at site HC32 partially remagnetized with a reverse polarity magnetization, with the degree of remagnetization increasing with increasing proximity to the contact. Although the characteristic magnetization of the flow sampled at site HC33 is also of reverse polarity, the anonymously shallow inclination for this flow was significantly different to be readily resolved in

Table 4
Summary of positive reversal tests from the Hamblin–Cleopatra Volcano

Traverse	*D/I*	α_{95}/κ	n/n_T	Initial $2\theta_{63}$	k_n/k_r	Critical angle	Actual angle	Class
Cleopatra Wash								
Normal	346/55	4.3/53	22/56	22.2	2.9	7.8	4.9	B
Reverse	157/−56	6.5/18	29/56	38.1				
Southern								
Normal	6.2/55	20/151	2/12	18.6	3.1	16.3	14.2	C
Reverse	161/−57	17/48.5	4/12	47.6[a]				
Block Tests								
Cleopatra Lobe								
Normal	341/55	4.4/32	34/96	56.6	1.4	6.2	2.5	B
Reverse	158/−54	4.4/23	47/96	47.2				
Central Core								
Normal	8.9/60	6/123	6/18	40.2	4.8	15.7	7.6	C
Reverse	176/−57	15/26	5/18	66.4[a]				

[a] These means reflect exclusion of some sites because they were greater than $2\theta_{63}$ from the mean of the entire block (in this case 33.9 degrees).

vector diagrams of samples from site HC32. The remaining contact tests were either of insufficient detail or were conducted on host rocks with magnetizations of identical polarity too similar in direction to those of cross-cutting intrusions.

The southernmost traverse of the Cleopatra Lobe is the Boathouse Cove traverse, which is located within a fault-bounded block that defines the southwest tip of the eastern half of the volcano (Figs. 2 and 6a). All eight sites are in flows and each yielded well-grouped site means. Seven of these sites have a north-northwest to west declination and positive inclination magnetization (Table 2). Three sites were rejected from the in situ mean for the Cleopatra Lobe, using $2\theta_{63}$ statistical criteria (where θ_{63} is the angular standard deviation, which describes the angle about the true mean direction that includes 63% of the directions used to determine the mean). All samples behaved well during AF demagnetization, with excellent agreement between thermally demagnetized and AF demagnetized specimens. No dikes are exposed along the traverse, so no contact tests could be performed. Given that only one of the eight sites yielded a negative inclination magnetization, no reversal test was conducted.

The grand mean determination for the Cleopatra Lobe is based on 81 accepted sites out of 96 total sites collected along the four traverses (Table 5). We followed a two-tier approach to reject anomalous site mean data. A total of 10 sites were rejected, at the traverse level, because their in situ directions were greater than two angular standard deviations from the initial traverse mean determination. An additional five sites were rejected when all of the

Table 5
Summary of paleomagnetic data, Hamblin–Cleopatra Volcano and related rocks

Traverse	In situ				Structural correction[a]		Stratigraphic correction		
	D/I	α_{95}/κ	n/n_T	$2\theta_{63}$	*D/I*	α_{95}/κ	*D/I*	α_{95}/κ	n/n_T
Cleopatra Lobe:									
Cathedral Cove	338/52	5.1/48	18/20	31.4	4.7/52	5.1/48	10/45	6.5/28	19/20
Cleopatra Wash	341/56	4.1/25	51/56	46.0	12/53	4.1/25	34/40	4.1/25	51/56
Southern Traverse	349/57	10/38	6/12	44.6[b]	10/41	14/13	8/53	13/17	8/12
Boat House Cove	322/45	17/14	6/8	61.7[b]	346/51	16/14	342/65	21/6.9	8/8
Central Core:	3/59	6.8/42	11/18	84.1[b]	58/78	7/42	358,30	10/20	12/18
Hamblin Lobe:									
Hamblin Mountain	243,75	18/8.3	9/10	73.1	–	–	223,49	21/6.1	9/10
Sandy Cove	168,58	6.5/30	18/21	64.5	–	–	189, − 55	9.5/14	18/21
Wilson Ridge pluton:	337/64	12/11	13/14	57.6	–	–	–	–	–
West End Wash/Callville Mesa:	32/44	5.1/31	27/27	29.1	–	–	–	–	–
Triassic Chinle:	37/35	6.7/29	4/4	30.1	–	–	51,22	6.7/29	5/5
Block means:									
Cleopatra Lobe	339/54	3.1/27	81/96	33.9	9/53	3.1/27	24/44	3.8/18	85/96
Central intrusive	3/59	6.8/42	11/18	84.1[b]	58/78	6.8/42	1.5/28	7.3/36	11/18
Hamblin Lobe	168/−58	6.5/29	18/29	30.1	–	–	185/−55	9.7/13	19/29

[a] The structural correction is constant for a given traverse, the α_{95} and κ values are identical to the in situ values of these parameters.
[b] These means reflect exclusion of some sites because they were greater than $2\theta_{63}$ from the mean of the entire block (in this case $2\theta_{63} = 33.9°$).

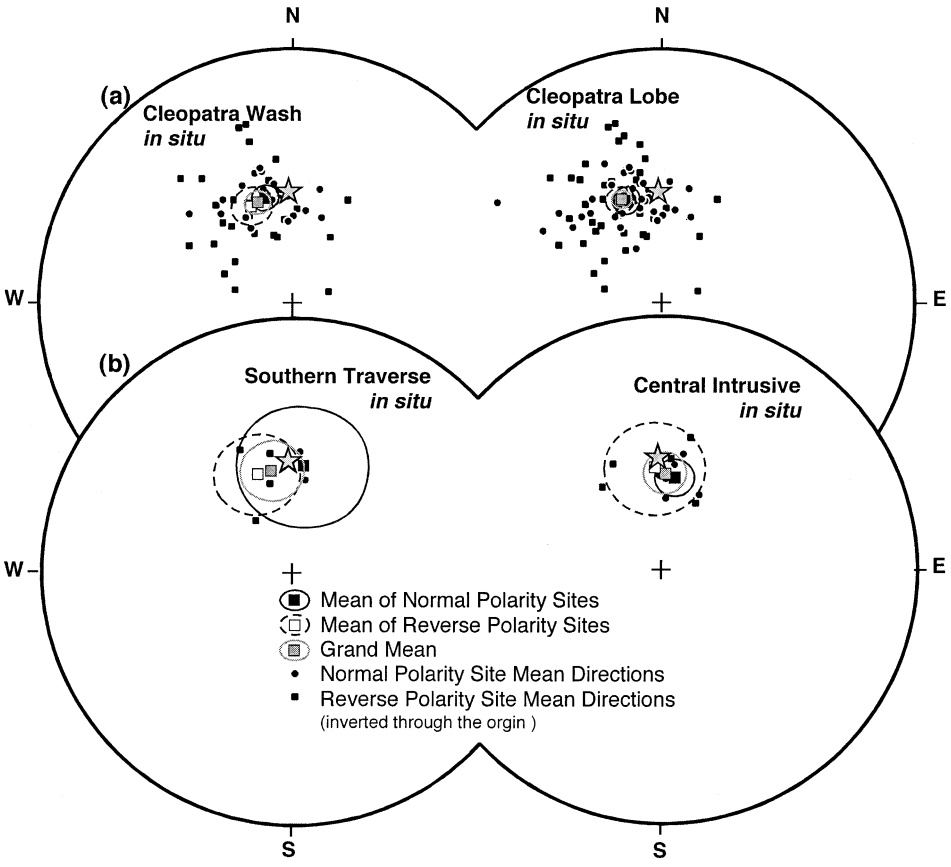

Fig. 8. Equal-area projections showing populations of in situ site mean directions that provided positive reversal tests (Table 4). Reverse polarity mean directions (squares) have been inverted through the origin of the projection and are plotted on the lower hemisphere. (a) Normal and reverse polarity directions, associated means and grand mean of results from the Cleopatra Wash Traverse are plotted on the left. The results for the entire Cleopatra Lobe are plotted on the right. (b) Normal and reverse polarity means of results from the southern traverse are plotted on the left. The normal and reverse polarity means of results from the central intrusive core are plotted on the right. The star is the middle Miocene reference direction of Mankinen et al. (1987).

sites were averaged into a grand mean for the entire lobe and their mean directions were found to be greater than two angular standard deviations from the mean. Inversion of reverse polarity directions to normal polarity results in a well-grouped mean of NNW declination (339°) and moderate positive inclination (+54°) ($k = 27$, $\alpha_{95} = 3.1°$ (Table 5)). The ensemble of 81 accepted sites for the Cleopatra Lobe passed a reversal test (Class B) (Table 4; Fig. 8).

3.2. Central intrusive core

The central intrusive core of the Hamblin–Cleopatra Volcano was sampled along Boulder Wash (Central traverse) and included relatively altered extrusive, hypabyssal intrusive and host contact rocks of the intrusive core and altered volcanic rocks of the middle lobe (Fig. 6). Hydrothermal alteration of these rocks is apparent in the ubiquitous sericitization of feldspars and overall leaching of pigment phases from the rock groundmass. Eighteen sites were collected from dikes and flows, two conglomerates and one coarse, poorly sorted, lithic arenite. In total, only about half of the samples from this traverse displayed stable end-point behavior and only 16 sites provided interpretable results. A total of 11 sites were used in the final in situ mean determination (Tables 2 and 5). No contact tests were performed because the rocks at contacts were typically highly altered and the field relations between intrusions and host rocks were not straightforward. The conglomerates were not well-suited for conducting conglomerate tests because clast sizes were too small. The sites used in the in situ mean determination from this traverse passed a reversal

Fig. 9. Equal-area stereographic projections of in situ, dike-tilt corrected and flow-tilt corrected site mean directions, associated grand means for each population, and the expected middle- to late-Miocene normal polarity field directions, as discussed in the text. Normal polarity site directions are plotted on the lower hemisphere as solid circles, reverse polarity site directions are plotted on the upper hemisphere as open squares. (a) Results from the Cleopatra Lobe. (b) Results from the Central Intrusive core. (c) Results from the Hamblin Lobe. (d) Results from the Hamblin Wash traverse (Wilson Ridge pluton). (e). In situ mean direction of results from the Callville Mesa/West End Wash traverses and the in situ mean direction and associated tilt corrected mean direction from the Triassic Chinle traverse. The associated tilt corrected mean direction from the Triassic Chinle traverse and the associated expected directions are also shown.

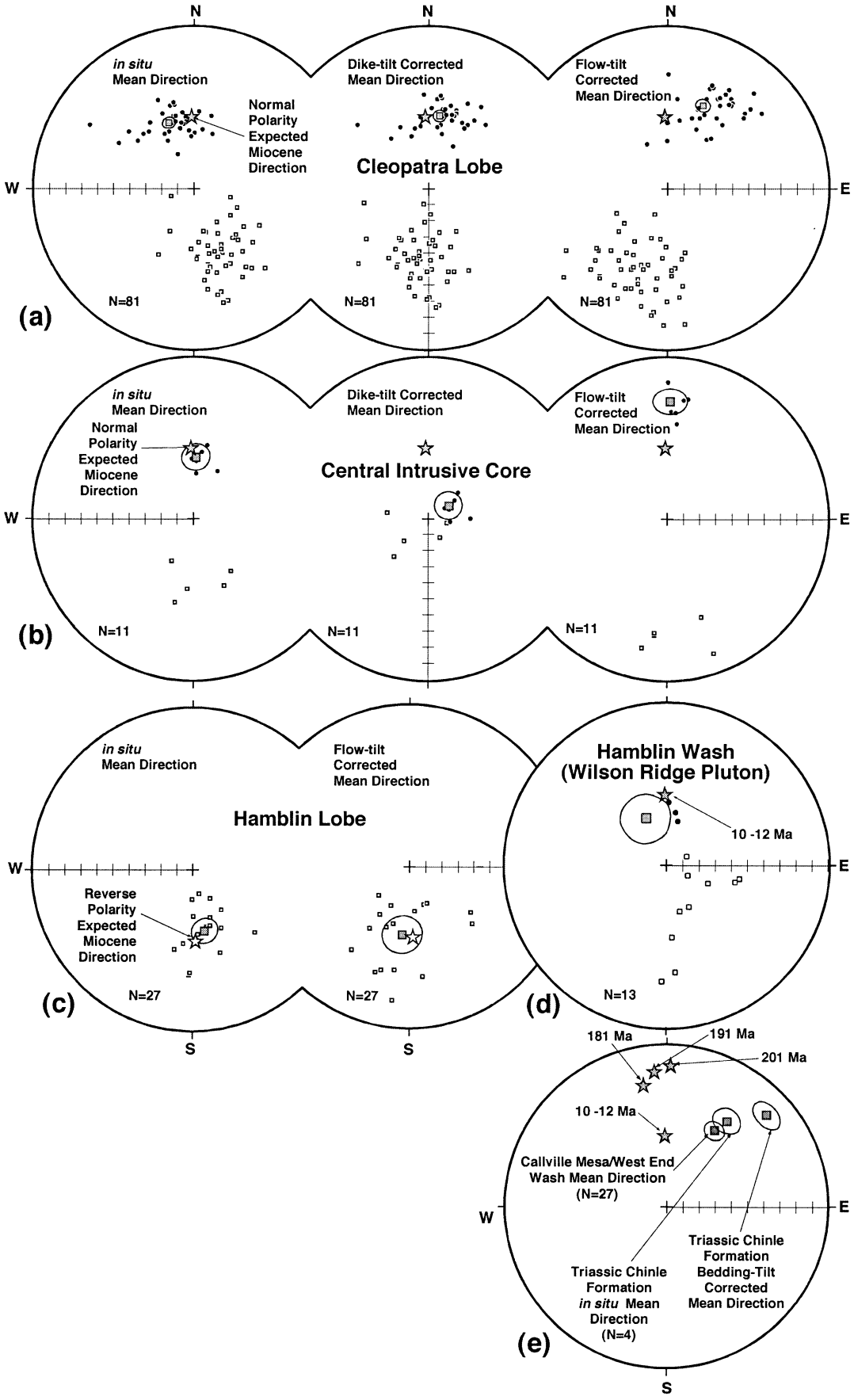
N
W
E
S
in situ
Mean Direction
Normal
Polarity
Expected
Miocene
Direction
Dike-tilt Corrected
Mean Direction
Flow-tilt
Corrected
Mean Direction
Cleopatra Lobe
N=81
(a)
Central Intrusive Core
N=11
(b)
Hamblin Lobe
Reverse
Polarity
Expected
Miocene
Direction
N=27
(c)
Hamblin Wash
(Wilson Ridge Pluton)
10 -12 Ma
N=13
(d)
181 Ma
191 Ma
201 Ma
10 -12 Ma
Callville Mesa/West End
Wash Mean Direction
(N=27)
Triassic Chinle
Formation
in situ Mean
Direction
(N=4)
Triassic Chinle
Formation
Bedding-Tilt
Corrected
Mean Direction
(e)

Fig. 9.

test (Class C) (Table 4). For this area, the timing of magnetization acquisition and, thus, the resolved mean are of uncertain age, as the magnetizations could reflect considerable chemical alteration and, therefore, are not representative of the primary magnetizations. The accepted in situ results are statistically indistinguishable from expected mid- to late-Miocene field directions (Fig. 9).

3.3. Hamblin Lobe traverses

Within the Hamblin Lobe, two traverses were made—Hamblin Mountain traverse (10 sites) and the Sandy Cove traverse (21 sites). The Hamblin Mountain traverse yielded 10 statistically well-defined site means of either intermediate directions or reverse polarity; the Sandy Cove traverse yielded entirely reverse polarity site means (Table 2). Similar to the results from the Cleopatra Lobe, no more than two magnetizations were isolated in progressive demagnetization treatments. Most sites yielded well-grouped magnetizations at the site level, based on stable end-point behavior (Fig. 7a). Only one site (HM1) of the Hamblin Mountain traverse yielded a mean direction that is consistent with a normal or reverse polarity Miocene field (in this case reverse). Seven sites yield means with well-grouped southwest to south-southwest declination and moderate positive inclinations (Table 2) that are anomalous with respect to data from the Sandy Cove traverse and elsewhere in the volcano. As a conservative approach, all sites from the Hamblin Mountain traverse are rejected in the final mean determination for the Hamblin Lobe. From the Sandy Cove traverse, three sites were excluded, because their means were greater than $2\theta_{63}$ from the initial mean determination, leaving a total of 18 means for the entire Hamblin Lobe. Given that the accepted sites are of the same polarity, no reversal test could be performed. Also, because all sites were in flows and pyroclastic deposits, the only magnetization test that could be performed was a conglomerate test at site SC60 (Fig. 7b). Well-rounded, monolithologic clasts from this site yielded random magnetization directions at a 95% confidence level, signifying the preservation of magnetization that predates disruption of the deposit from which the clasts were derived. As with the central intrusive core, the in situ group mean direction from the Hamblin Lobe is statistically indistinguishable from mid- to late-Miocene expected field directions (Fig. 9c).

3.4. The Wilson Ridge intrusive suite

At the northern end of Hamblin Bay (Hamblin Bay Wash traverse), 16 dikes of the northernmost Wilson Ridge intrusive complex were sampled. Map relations suggest that the northern part of the dikes have experienced significant counterclockwise rotation consistent with sinistral shear along the Hamblin Bay fault (Anderson et al., 1994) (Fig. 2). We were not able to perform baked contact tests because of poor contact exposures and alteration of host rocks. Thirteen acceptable site means were obtained, with magnetizations of both normal and reverse polarity but variable direction recorded. Several site mean directions are consistent with a large-magnitude, post-magnetization acquisition counterclockwise rotation that is in agreement with the deflection of dike trends, from north–south to roughly east–west, as the Hamblin Bay fault is approached. For example, site HW46 yielded an in situ mean direction with a moderate negative inclination (−54°) and east-southeast declination; this direction is discordant from the expected reverse polarity direction by about 70–80°. Given the lack of a bipolar distribution of the data (Table 2), a reversal test was not applied to the data. Although the age of these magnetizations is not unequivocally established, the 13 sites used in determining a mean direction yield a result that is clearly discordant from Miocene expected directions (Table 5; Fig. 9d).

3.5. Triassic Chinle Formation

Four sites were collected in the four best-exposed and most hematite-cemented beds of tilted Triassic Chinle Formation strata located north of the Boulder Wash traverse and northwest of the Hamblin Bay Fault (Fig. 2). All samples behaved uniformly during thermal demagnetization, which clearly revealed the presence of two magnetizations of higher unblocking temperature. An in situ magnetization of northeast declination and moderate to shallow positive inclination was unblocked above about 610°C and decayed to the origin in vector diagrams (Fig. 6). Additional sampling of these rocks might better characterize these magnetizations; however, on the basis of the internal consistency of the results, we suggest that these data are consistent with modest clockwise rotation ($57 \pm 6°$) in comparison with a Late Triassic reference direction (Van der Voo, 1993).

3.6. West End Wash/Callville Mesa volcanic centers

The West End Wash and Callville Mesa basalt sequences, which crop out west of the Hamblin Lobe (Fig. 1), and are slightly younger than rocks of the Hamblin–Cleopatra Volcano, were collected as two separate traverses. Rocks from the Callville Mesa and West End Wash volcanic centers, which are adjacent to one another, provided remarkably uniform demagnetization results at the site-level (Table 2). Sample directions were readily defined in the stable-end-point behavior that routinely required AF demagnetization treatments of up to 120 mT (Fig. 10). Samples with median destructive fields greater than about 70 mT required further thermal demagnetization to 580°C and in all cases the demagnetization results were consistent with partially AF demagnetized samples. All 27 sites from these two traverses, within flat-laying basalt flows, yielded site mean directions of northeast declination and shallow to moderate positive inclination (Table 3; Fig. 10). The grand mean results for the two sequences are statistically distinguishable, with the Callville Mesa mean about 19°

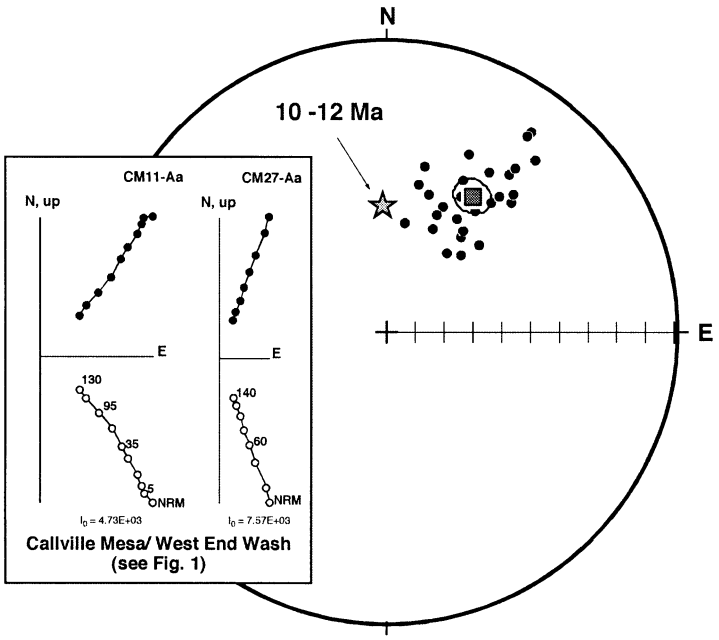

Fig. 10. Paleomagnetic results from the Callville Mesa/West End Wash traverses (located at Callville Mesa: see Fig. 1). Equal-area, lower-hemisphere projection and associated demagnetization diagrams of results both traverses. Representative orthogonal demagnetization diagrams (Zijderveld, 1967) from the Callville Mesa traverse.

shallower in inclination than the West End Wash mean. Given the unusually low dispersion of site mean directions for each traverse and the overall directions of magnetization from these rocks, it is likely that neither sequence of anomalous, uniform polarity results represents a sufficiently robust sampling of the geomagnetic field.

3.7. Summary of paleomatic results

Mean directions of magnetization obtained for particular traverses as well as separate structural domains typically have high levels of precision, as defined by Fisher's precision parameter, k (Table 5; Figs. 5–8). Among the domains studied, the data from the Cleopatra Lobe represent the largest number of independent samplings of the geomagnetic field. The in situ grand mean declination of 338° differs from expected, mid- to late-Miocene field directions (e.g. at 10 Ma, $D = 356°$ $I = 54°$; Irving and Irving, 1982) by some 10° in a counterclockwise or westward sense. The in situ inclination is identical to expected values within resolution of the data (Table 5). Data from the Cleopatra Lobe, as well as two specific traverses within it, pass reversal tests (Class C or better; Table 4) suggesting that the rocks sampled from these areas record at least two polarity chrons, supporting the assumption that our data set probably averages paleosecular variation. Together with dike contact and conglomerate tests, the data indicate a primary nature to the magnetizations. The in situ means from the central intrusive core and the Hamblin Lobe (Table 6) are statistically indistinguishable from expected

Table 6
Summary of tilts and rotations, Hamblin–Cleopatra Volcano and related rocks

Block name	Identified mean	Mean direction		Co-latitude	Discrepancies[a]		Tectonic interpretation
		D/I	α_{95}/κ		$R \pm \Delta R$	$F \pm \Delta F$	
Hamblin–Cleopatra Volcano:							
Cleopatra Lobe	Dike corrected	009/53	3.1/27	56.4°	13° ± 3.2°	3° ± 4.3°	20° tilt (see text)
Intrusive core	In situ	003/59	6.8/42	50.2°	7° ± 7.3°	−3° ± 6.7°	no tilt, no rotations
Hamblin Lobe	In situ	348/58	6.5/29	51.3°	−8° ± 7.3°	−2° ± 6.6°	no tilt, no rotations
Associated traverses:							
Wilson Ridge pluton	In situ	337/64	12/11	44.3°	−19° ± 14°	−6° ± 9.9°	5° CCW rotation
Callville Mesa–West End Wash	In situ	032/44	5.1/31	64.2°	36° ± 5.4°	12° ± 7.2°	see text
Triassic Red Beds	Tilt corrected	051/22	6.7/29	78.5°	57° ± 6.2°	−1° ± 12°	50° CW rotation

[a] Calculated in directional space where R is the difference between observed and the expected declination and F is the difference between observed and expected inclination (positive values of R represent clockwise (CW) rotations). Colatitude is the angular distance between the site and the mean paleopole position for the block.

middle- to late-Miocene directions. However, the lack of definitive field tests for the age of magnetization for results from the central intrusive core makes it less straightforward to assign a primary age to the magnetization recorded. Within the Hamblin Lobe, results from the conglomerate test at site SC60, Sandy Cove traverse, suggest that these rocks have not experienced widespread remagnetization. In addition, the absence of normal polarity site means, with the exception of the anomalously magnetized flows of the Hamblin Mountain traverse, may imply a lack of sufficient averaging of the geomagnetic field. Data from several of the dikes at the northernmost end of the Wilson Ridge intrusive complex and the albeit small number of sites in the Chinle strata differ from their respective expected directions for these rocks (Fig. 9) and imply that the rocks in these sampling area have been substantially rotated, consistent with geologic field evidence (Anderson et al., 1994).

Not all independent volcanic deposits or intrusions of the Hamblin–Cleopatra Volcano have been, or could be, sampled in this study. Our sampling strategy represented an attempt to meet the basic paleomagnetic requirement of assessing independent deformation of discrete and structurally coherent blocks, all the while attempting to sample the freshest, most intact and best-exposed materials possible. The likelihood of repetitive sampling of a single flow or dike across two (or more) separate traverses, and thereby introducing a bias into the data set, is negligible because the conical morphology of a strato-volcano limits the width of the areal distribution of a single eruptive flow event (Hackett and Houghton, 1989). With the possible exception of the southern traverse ($N = 12$ sites) of the Cleopatra Lobe (Fig. 2), the traverses are located in sufficiently different positions with respect to the core of the volcano to avoid repetition of sampling of any one dike or flow. Moreover, most traverses were conducted to maximize vertical coverage through the volcanic pile, thereby avoiding repeated sampling of temporally identical eruptive events. The observed dispersion of individual site directions, including the dual-polarity nature, from the rocks of the Hamblin–Cleopatra volcano strongly supports an interpretation that a primary magnetization is preserved and that these rocks have not been thermally or chemically remagnetized in some widespread alteration event. We interpret the paleomagnetic data, particularly from the Cleopatra Lobe, to have sufficiently averaged paleosecular variation during the middle- to late-Miocene and suggest that the data obtained here form a strong base from which we can assess the role of vertical axis block rotation along this part of the LMFS.

4. Discussion

Paleomagnetic methods are an excellent technique for quantifying estimates of either tilt about a horizontal axis or vertical-axis rotations of deformed rocks. The accuracy of these estimates, however, is strongly dependent on the reliability of any structural corrections applied to the data. Generally, such corrections involve removing tilt by rotating the paleomagnetic data about the present strike axis to restore the data to paleohorizontal. If this correction is applied in the context of a known kinematic framework, then assessment of any discrepancy between the corrected and the expected directions will provide insight into likely tectonic explanations. We have taken a somewhat unorthodox approach in attempting to resolve the issue of identifying the paleohorizontal datum for igneous rocks. After defining what we consider to be an appropriate datum, we discuss the tectonic importance of both tilting and vertical-axis rotation of rocks deformed along the LMFS. For clarity, we define the term 'tilt' as any rotation about a subhorizontal or horizontal axis. The term 'rotation' is defined as any rotation about a steep or vertical axis.

4.1. Tilt corrections and the paleohorizontal datum

Here we evaluate whether a realistic paleohorizontal datum can be established, considering further details of the geology of the Hamblin–Cleopatra Volcano. Thompson (1985) noted that dikes with traces sub-parallel to the trace of the western bounding fault of the Cleopatra Lobe (Fig. 2) are rarely vertical. Instead, their dips range from 60 to 70° and are consistently WNW. In contrast, dikes roughly orthogonal to the fault are generally sub-vertical. A total of 48 dikes located near the fault strike within 0–35° of the fault trace (i.e. these strikes vary between 210 and 175°) and define a mean normal that plunges 24 to 080° (corresponding to a mean strike and dip of 170, 66° west dip; Fig. 11a). Assuming the dike swarm of the Cleopatra Lobe was part of a radial system from a central cone and that most of the dikes originally had subvertical walls, it is possible to restore the dikes to a sub-vertical orientation by back-tilting them 24° about the mean strike (170°) of non-vertical dikes. Applying this partial, or 'dike-tilt' correction to the paleomagnetic data from rocks of the Cleopatra Lobe, the dike-tilt corrected mean is $D = 009°$, $I = 53°$. In contrast, applying the traditional stratigraphic-tilt corrected (removing tilt by rotating the data about the strike axis to restore the bedding to horizontal) resulted in a mean of $D = 024°$, $I = 44°$. The dike-tilt-corrected mean has a more north-directed declination, closer to expected middle- to late-Miocene field directions (Fig. 9). The dike-tilt correction may be a more realistic treatment of the data than application of simple stratigraphic tilt corrections, which would vary depending on sampling location. Given that this is a single, uniform correction (applied to all the site means of a particular block), the significance of the test cannot be evaluated.

Another approach to evaluating proper tilt corrections involves consideration of the distribution of dip directions of the flows of the Cleopatra Lobe. Assuming that the center of the radial dike swarm (Fig. 2) marked a topographically high edifice, the dip directions of flows should be radial

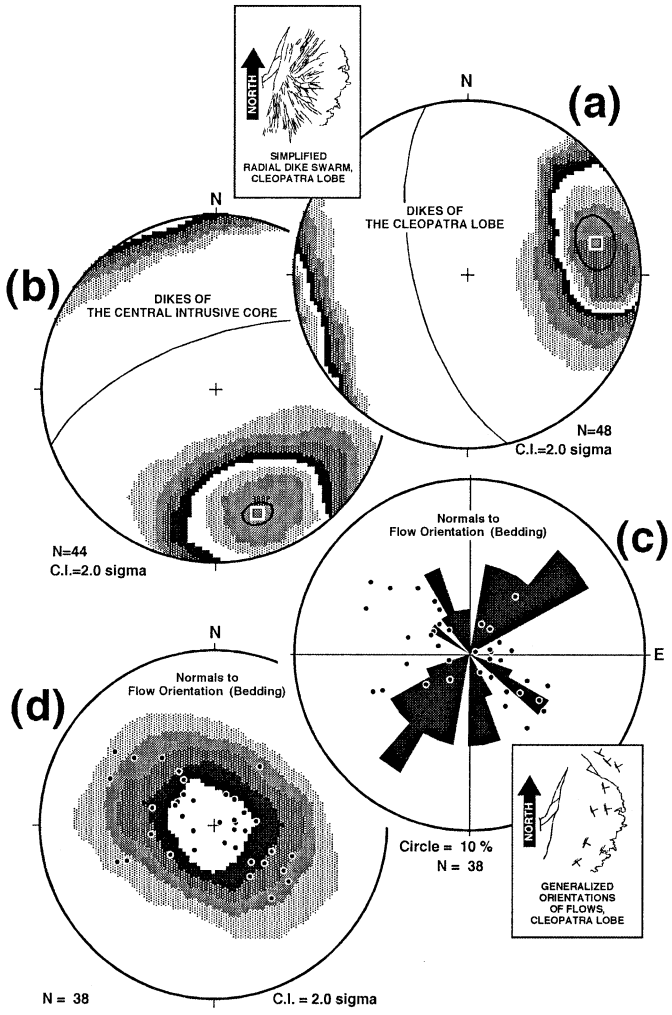

Fig. 11. Dikes and flow orientation data for the Hamblin–Cleopatra Volcano. The radial dike swarm of the Cleopatra Lobe is shown in the upper left inset (Thompson, 1985) and the orientations of lava flows of the Cleopatra Lobe are shown in the lower right inset (Anderson, 1973). (a) Equal area, lower-hemisphere projection of the mean (white square) of normals to dikes of the Cleopatra Lobe found near the trace of the Hamblin Bay Fault (Fig. 2), and the associated 95% cone of confidence determined by Fischer (1953) statistics, the contours of dike normals are also shown (method of Kamb (1959)). (b) Equal area, lower-hemisphere projection of the mean of normals to dikes of the central intrusive core that are sub-parallel to the Hamblin Bay Fault, the contours of dike normals are also shown. All dike data from Thompson (written communication, 1995). (c) Rose diagram of bedding strikes of flows in the Hamblin and Cleopatra Lobes, and equal-area stereographic projection of normals to bedding planes. (d) Equal area, lower-hemisphere projection of normals to bedding of flows in the Hamblin and Cleopatra Lobes with associated Kamb contours. All bedding data taken from Anderson (1973) or measurements made during this study.

from the edifice and roughly parallel to dike trends. We compared the observed in situ dip data with predicted dip data (Fig. 12) based on a conical distribution, to evaluate the importance of the observed non-conical geometry of the Cleopatra Lobe. In situ dip directions do not display a radial geometry (Fig. 11c and d). Observed strikes from locations that lie north-northeast or south-southwest of the central edifice have more north–south strikes than would be expected for the assumed conical morphology (Fig. 11c). The observed distribution of strike data is consistent with an elongate edifice sub-parallel to the trace of the main bounding fault or with rigid-block tilting about an axis sub-parallel to the same bounding fault. To test the validity of the dike-tilt correction, we used this correction to restore the flow attitude data to a pre-tilt configuration. We also corrected the in situ flow attitude data about an axis sub-parallel to the trace of the Hamblin Bay fault, which bounds the western margin of the Cleopatra Lobe. An ideal correction would bring the observed dip directions into agreement with a radial distribution of dip directions. Any realistic correction would not result in beds that dip towards the central edifice, at high angles to the paleohorizontal datum. We compared expected dip azimuth values with: (a) observed dip azimuth, (b) dip azimuths after rotating the flow orientation data 24° about a horizontal axis trending 170° (the dike corrections), and (c) dip azimuths after back-tilting the data 20° about a horizontal axis trending 208° (the fault correction). This analysis (Fig. 12) revealed that a rotation about a horizontal axis sub-parallel to the fault restores a conical morphology of flow distribution about the central edifice marked by the

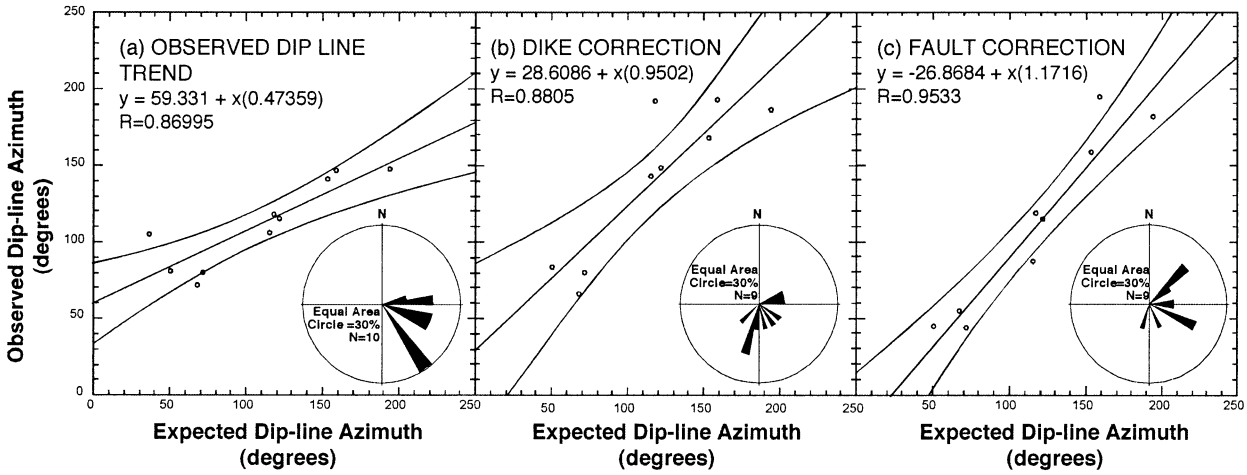

Fig. 12. Plots of expected dip-azimuth versus observed or modeled dip-line azimuth value. The observed dip-line azimuth was determined from the observed field orientations. To produce these plots, these data were first 'un-tilted' about the same axis used to 'un-tilt' the radial dike swarm. The final plot was produced by 'un-tilting' the observed dip line azimuth about a horizontal axis that is sub-parallel to the trend of the Hamblin-Bay fault. The best-fit linear regressions are shown along with their associated 95% confidence interval estimates.

locus of radial dike intersections. Linear, first-order, least-squared regressions yield correlation coefficients of 0.870, 0.881 and 0.953, for the observed, dike corrected, and fault-corrected bedding orientation data, respectively. The correction that results in a radial dip line morphology, supporting the possibility of moderate, east to east-southeast side down rigid-block tilting of the Cleopatra Lobe, appears to be the most accurate restoration of flow orientation data for the Cleopatra Lobe.

In summary, the uniform application of simple, stratigraphic tilt corrections to the paleomagnetic data from rocks of the Hamblin–Cleopatra Volcano is considered inappropriate. We argue that a tilt correction based on dike orientations is realistic for the Cleopatra block and is consistent with moderate fault-related, rigid-body tilting in the area. Overall, our results differ from those of Ron et al. (1986), who concluded that stratigraphic tilt corrections are inappropriate for flows of the volcano, yet for a different reason. They arrived at this conclusion by comparing precisions of tilt corrected data with in situ data. Noting a decrease in precision as a result of application of stratigraphic corrections, they proposed that the in situ data characterize the middle- to late-Miocene paleomagnetic field and did not consider the possibility that at least parts of the volcano had been significantly tilted as a consequence of normal faulting.

Duebendorfer et al. (1998) emphasize that Miocene east-side down tilting is widespread in the Lake Mead area and is genetically related to deformation on kinematically linked high-angle normal, strike-slip transfer, and west-dipping detachment faults that underlie the crust in the area. The transfer faults adjust for contrasts in the distribution of extension on the high-angle normal and west-dipping detachment faults. Although the paleomagnetic data reported here are consistent with modest tilting of some blocks, they cannot be interpreted to support regional-scale, uniform east-side down tilting. Also, if the 20 km southwest displacement of the Hamblin Lobe relative to the Cleopatra Lobe (Fig. 2) resulted from transfer-fault adjustment for slip on a detachment fault beneath the volcano that dipped as gently as 5°, two effects should be apparent: (1) rocks in the Hamblin Lobe should be tilted eastward more than the Cleopatra Lobe as a result of tilting on high-angle faults that fed into the detachment fault, and (2) the rocks in the Hamblin Lobe should be about 1.5 km structurally lower than the Cleopatra Lobe as a result of displacement on the detachment fault. Because neither of these effects is apparent, we suggest that the kinematically integrated faulting model is invalid and that the two volcanic blocks were separated by a process of structural rafting on a ductile-flowing substrate, as proposed by Anderson et al. (1994).

4.2. Regional strike-slip faulting and block rotations

The right-lateral Las Vegas Valley shear zone (LVVSZ) was active from 15 to 9 Ma (Fleck, 1970; Duebendorfer and Black, 1992; Duebendorfer and Simpson, 1994) and the left-lateral LMFS was active from 17 to 10 Ma, (Bohannon, 1984). Eruption of the Hamblin–Cleopatra Volcano (ca. 13.1 to about 10.1 Ma, Anderson et al., 1972, 1994), as well as the Callville Mesa/West End Wash basalts (ca. 11.5 to about 8.5 Ma, Feuerbach et al., 1991, Harlan et al., 1998), occurred during the interval when these two major strike-slip faults were active. This overlap in timing suggests that some vertical axis rotation may have taken place during volcanism and slip along these regional fault systems. The magnitude and spatial variability of block rotations associated with the southeast termination of the LVVSZ have been evaluated by Sonder et al. (1994), as further discussed below. The data presented here are

interpreted to indicate that rocks along the LMFS have experienced heterogeneous tilting and rotation.

The variability of both tilts and rotations of rocks within the LMFS may be supported by the overall dispersion of corrected and uncorrected block mean directions (Table 5; Fig. 9). We can attempt to identify statistically significant tilts and rotations by comparing specific block means with Miocene field directions for this area (Table 6). The in situ paleomagnetic data were used for all blocks except for the Cleopatra Lobe (as discussed above) and the locality where Triassic Chinle strata were sampled. For the purpose of interpreting the relative importance of tilts or rotations, in both of these cases, a structural correction of some type should be applied to these data. The east-down tilt of the major, structurally intact Cleopatra Lobe is based on the dike-tilt correction described above. After removal of this tilt, the declination discrepancy (R) suggests about 13° of clockwise rotation of the entire Cleopatra Lobe. It should be noted, however, that if the tilt estimate is about 4° too high, then the block mean direction would be statistically indistinguishable from expected directions. We contend, therefore, that our results are consistent with dip-slip on parts of the LMFS resulted in moderate, local tilting (about 20°, down to the east, for the Cleopatra Lobe) during Cenozoic extension and strike-slip faulting. Despite the fact that tilt corrections cannot be evaluated as rigorously, both the intrusive core and the Hamblin Lobe yield data that are not suggestive of any significant tilt or rotation. The data from the Wilson Ridge dike complex appear to be rotated in a manner consistent with the mapped oroclinal flexure of these intrusions south of the Hamblin Bay Fault (Fig. 2), but these results are not statistically robust. The results from the Triassic Chinle strata, located northwest of the Cleopatra Lobe (Fig. 2) are rotated, significantly, in a clockwise fashion. Given that the magnetization in these rocks pre-dates Neogene deformation, it is not clear if all or part of this rotation is a result of deformation along the LMFS. Finally, we defer from placing any tectonic significance on the data from the Callville Mesa/West End Wash basalts. We interpret the Callville Mesa/West End Wash sequence to have been erupted over a span of time that was insufficient in length to adequately average the paleomagnetic field; the data from these volcanic centers probably represent a partial record of paleosecular variation.

Previous paleomagnetic investigations have tested the distribution and kinematics of rotations associated with the LVVSZ and the LMFS and have led to contrasting interpretations. Sonder et al. (1994) noted clockwise rotations that are consistent with oroflexural map patterns in Miocene sedimentary rocks along the LVVSZ. Rotations increase with proximity to the shear zone and reach values of 100° within blocks 2–4 km wide adjacent to the zone. They interpreted this rotation gradient as shear-related deformation of a thin viscous (highly plastic), mechanically decoupled upper crust in which the rotations were controlled by the intrinsic rheology of the crust and the dimensions of the shear zone. They argued that the data recluded wholescale rigid-block rotation as a deformation mechanism. In contrast, limited paleomagnetic data from rocks of the Hamblin–Cleopatra Volcano along the NE-striking left-slip LMFS were interpreted by Ron et al. (1986) as reflecting rigid-block deformation of blocks bounded by north striking right-slip faults that rotated counterclockwise with the blocks in a domino style. Anderson et al. (1994) suggested, on the basis of field-determined dike orientations, that strong disharmonic steep-axis bending in the Wilson Ridge pluton directly south of the Hamblin Bay strand of the LMFS is greater than that in the Hamblin Lobe north of the fault. They interpreted the strong bending as continuous ductile strain associated with north–south shortening rather than proximity to the major strike-slip fault splay. They suggested a similar interpretation for the significant clockwise rotation of the sedimentary rocks along the easternmost part of the LVVSZ, reported by Sonder et al. (1994). We now consider which, if any, of these interpretations is consistent with the paleomagnetic data reported here.

Our new paleomagnetic data suggest that each individual block along the LMFS may have its own unique rotation characteristics. Only three of the six blocks considered have experienced any statistically discernable rotations. For the Chinle strata, the rocks sampled are considerably older than deformation along the fault system and could have been rotated during thrust-belt contraction in the Mesozoic. The largest and most intact block, the Cleopatra Lobe, is not appreciably rotated; in fact, we believe that our analysis of dike orientations and overall geometry of lava flow dips conclusively demonstrates about 20° of east-side down tilting of the Cleopatra Lobe. Clearly, these results are inconsistent with the model of uniformly rotated blocks and the absence of block tilting, as proposed by Ron et al. (1986).

Keeping in mind that the rocks we studied are adjacent to a different fault than those studied by Sonder et al. (1994), and are mainly igneous rather than sedimentary, our results seem to lack a suggestion of a shear-related displacement gradient adjacent to the LMFS. Anderson et al. (1994) noted, on the basis of dike orientations, a similar lack of displacement gradient in the Hamblin Lobe. Large blocks such as the Hamblin and Cleopatra Lobes seem to have remained relatively intact and to have escaped strong internal bending deformation, despite having been displaced from one another by about 20 km (Fig. 2). This rather passive response contrasts sharply with the strong rotational strain in the north part of the Wilson Ridge pluton and in the sedimentary rocks along the east part of the LVVSZ, and highlights the strong heterogeneity of the total strain field, as emphasized by Anderson et al. (1994).

5. Conclusions

Understanding the roles of different types of faults common

to the Basin and Range province of the western Cordillera must be largely based on detailed mapping of field relationships. Paleomagnetic data, when of a sufficiently robust nature, can provide quantitative insights into the kinematics of these fault zones. In strike-slip systems, without piercing points to resolve absolute offsets, paleomagnetic data can place estimates on the sense and magnitude of rotations of crustal material. Within such systems it may be difficult to accurately reconstruct piercing points to resolve such rotations directly from field based observations.

The paleomagnetic data from the Hamblin–Cleopatra Volcano and related rocks support several conclusions. Rotations of blocks within the sampled part of the LMFS are either too minor to be detected by paleomagnetic techniques or, where statistically definable, are inconsistent from one block to the next. The Cleopatra Lobe was tilted about 20° in a south-east-down sense after volcanism, and the data do not support appreciable vertical axis rotation. Although strike-slip faulting is an undeniably important component of Basin and Range extension at this latitude (e.g. the Garlock fault, the Las Vegas Valley shear zone, and the LMFS), there is no compelling evidence that the strike-slip faults, and any attending vertical axis rotations, exerted a primary control on the observed style of deformation throughout the province at this latitude.

In a more regional sense, the data and discussion presented here provide insight into the mechanism of block translation during late Cenozoic extension in the Lake Mead area. There is little or no correlation between the distance of tectonic transport of the Hamblin Lobe from the Cleopatra Lobe and their respective tilting or current vertical structural levels. In fact, the Cleopatra Lobe, which is not known to have been transported at all, appears, on the basis of paleomagnetic data, to be tilted more to the east than the Hamblin Lobe and both are at essentially identical structural levels. We suggest that this lack of correlation is consistent with a model of tectonic rafting of the Hamblin Lobe on a ductile west-southwest flowing substrate. The structure of the Frenchman Mountain block (Fig. 1), which lies over 30 km to the west and has been tectonically transported over three times as far as the Hamblin Lobe (Duebendorfer et al., 1998), exhibits similar geologic relations with respect to its tectonic source area (Anderson, 1996) and, thus, a similar lack of correlation between magnitude of tilt and tectonic translation. These relations, and others considered by Anderson et al. (1994), lead us to favor a tectonic rafting model for major block translations in the Lake Mead area.

Finally, the paleomagnetic data are consistent with geologic mapping and dike-orientation data. Both indicate: (1) strong and abrupt contrasts in the amount, distribution, and sense of rotations adjacent to major strike-slip faults, and (2) inconsistency in the amount, distribution, and direction of tilting. Bohannon (1979, 1983) and Anderson et al. (1994) showed that much of the tilting in the Lake Mead area records shallow-axis Miocene and younger folding produced by north–south shortening—a major factor contributing to strain inhomogeneity in this region of extensional tectonics. We suggest that tectonic rafting of moderately to non-rotated structural blocks such as Frenchman Mountain and the Hamblin Lobe occurred in concert with north–south shortening that is recorded as both shallow-axis and steep-axis folds.

Acknowledgements

We thank Ralph Mason for his assistance in the collection of samples and for his aid in the completion of extensive laboratory measurements. We also thank Keith Thompson for having the foresight to collect invaluable orientation data on the dike swarm of the Cleopatra Lobe and the central intrusive core and for making these data available for our use. Financial support for field excursions and laboratory analysis was provided by the Explorer's Club and by the Department of Earth and Planetary Sciences at the University of New Mexico. National Science Foundation Grant EAR-8721264 provided partial support for the initial phases of this study. Additional support for laboratory analysis was provided by the UNM–Paleomagnetism Laboratory. Evaluations by Jimmy Diehl, Jim Evans and an anonymous reviewer are greatly appreciated and improved the manuscript.

References

Anderson, R.E., 1971. Thin skin distension in Tertiary rocks of southeastern Nevada. Geological Society of America Bulletin 82, 43–58.

Anderson, R.E., 1973. Large-magnitude late Tertiary strike-slip faulting, North of Lake Mead, Nevada. U.S.G.S. Professional Paper 794, 18pp.

Anderson, R.E., 1996. Structural relations between Las Vegas Basin and the Frenchman Mountain/Sunrise Mountain Block, Southern Nevada. University of Nevada, Las Vegas, Seismic Hazards in the Las Vegas Region, Program with Abstracts 17.

Anderson, R.E., Barnhard, T.P., 1991. Neogene strain incongruity at the Hamblin Bay Fault, Lake Mead, Nevada. Geological Society of America, Cordilleran Section, Abstracts with Programs 23, 3.

Anderson, R.E., Longwell, C.R., Armstrong, R.L., Marvin, R.F., 1972. Significance of K–Ar ages of Tertiary rocks from the Lake Mead region, Nevada, Arizona. Geological Society of America Bulletin 83, 273–288.

Anderson, R.E., Barnhard, T.P., Snee, L.W., 1994. Roles of plutonism, midcrustal flow, tectonic rafting, and horizontal collapse in shaping the Miocene strain field of the Lake Mead area, Nevada and Arizona. Tectonics 13, 1381–1410.

Angelier, J., Colletta, B., Anderson, R.E., 1985. Neogene paleostress changes in the Basin and Range; a case study at Hoover Dam, Nevada, Arizona. Geological Society of America Bulletin 96, 347–361.

Bohannon, R.G., 1979. Strike-slip faults of the Lake Mead region of southern Nevada. In: Armentrout, J.M., Cole, M.R., TerBest Jr, J. (Eds.). Cenozoic paleogeography of the western United States, Pacific Coast Paleogeography Symposium. Published by Society of Economic Paleontologists and Mineralogists, Pacific Section, Los Angeles, USA, pp. 129–139.

Bohannon, R.G., 1984. Nonmarine sedimentary rocks of Tertiary age in the Lake Mead regions, southeastern Nevada and northwest Arizona. U.S.G.S. Professional Paper 1259, 72pp.

Burchfiel, B.C., 1965. Structural geology of the Spector Range Quadrangle, Nevada, and its regional significance. Geological Society of America Bulletin 76, 175–191.

Calderone, G.J., Butler, R.F., Acton, G.D., 1990. Paleomagnetism of middle Miocene volcanic rocks in the Mojave–Sonora desert region of western Arizona and southeastern California. Journal of Geophysical Research 92, 10422–10426.

Cas, R.A.F., Wright, J.V., 1987. Modern volcanoes and volcanic centres. In: Volcanic Successions Modern and Ancient. A Geological Approach to Processes, Products and Successions. Allen and Unwin, London, Chapter 13, pp. 363–410.

Duebendorfer, E.M., Beard, L.S., Smith, E.I., 1998. Restoration of Tertiary deformation in the Lake Mead region, southern Nevada: the role of strike-slip transfer faults. In: Faulds, J.E., Stewart, J.H. (Eds.). Accommodation Zones and Transfer Zones: The Regional Segmentation of the Basin and Range Province. Geological Society of America, Boulder, CO, USA, Geological Society of America Special Paper 323, pp. 127–148.

Duebendorfer, E.M., Black, R.A., 1992. Kinematic role of transverse structures in continental extension; an example from the Las Vegas Valley shear zone, Nevada. Geology 20, 1107–1110.

Duebendorfer, E.M., Simpson, D.A., 1994. Kinematics and timing of Tertiary extension in the western Lake Mead region, Nevada. Geological Society of America Bulletin 106, 1057–1073.

Eaton, G.P., 1978. Tectonic environment of late Cenozoic Great Basin volcanism. EOS, Transactions, American Geophysical Union 59, 248.

Faulds, J.E., Geissman, J.W., Shafiqullah, M., 1992. Implications of paleomagnetic data on Miocene extension near a major accommodation zone in the Basin and Range province, northwestern Arizona and southern Nevada. Tectonics 11, 204–227.

Feuerbach, D.L., Smith, E.I., Walker, J.D., Tangeman, J.A., 1991. The transition from subalkalic to alkalic volcanism in the Lake Mead area of Nevada and Arizona; geochemical and isotopic constraints. Geological Society of America Abstracts with Programs 23 (2), 24.

Fischer, R.A., 1953. Dispersion of a sphere. Royal Society of London Proceedings A217, 295–305.

Fleck, R.J., 1970. Age and possible origin of the Las Vegas valley shear zone, Clark and Nye counties, Nevada. Geological Society of America Abstracts with Programs 2, 333.

Geissman, J.W., Harlan, S.S., Wawrzyniec, T.F., 1989. Research note: Strike-slip faulting and block rotation in the Lake Mead Fault System. Geology 17, 1057–1058.

Hackett, W.R., Houghton, B.F., 1989. A facies model for a Quaternary andesitic composite volcano; Ruapehu, New Zealand. Bulletin of Volcanology 51, 51–68.

Harlan, S.S., Duebendorfer, E.M., Deibert, J.E., 1998. New $^{40}Ar/^{39}Ar$ isotopic dates from Miocene volcanic rocks in the Lake Mead area and southern Las Vegas Range, Nevada. Canadian Journal of Earth Sciences 35, 495–503.

Irving, E., Irving, G.A., 1982. Apparent polar wander paths Carboniferous through Cenozoic and the assembly of Gondwana. Geophysical Surveys 5, 141–188.

John, B.E., Howard, K.A., 1994. Disharmonic drape folds in the highly attenuated Colorado River extensional corridor, California and Arizona. In: McGill, S.F., Ross, T.M. (Eds.), Geological Investigations of an Active Margin. Geological Society of America, Cordilleran Section, Annual Meeting, Guidebook. Geological Society of America, Boulder, CO.

Kamb, W.B., 1959. Petrofabric observations from Blue Glacier, Washington, in relation to theory and experiment. Journal of Geophysical Research 64, 1908–1909.

Kirschvink, J.L., 1980. The least-squares line and plane and the analysis of palaeomagnetic data. Geophysical Journal of the Royal Astronomical Society 62, 699–718.

Longwell, C.R., 1950. Tectonic theory viewed from the Basin Ranges. Geological Society of America Bulletin 61, 413–433.

Longwell, C.R., 1974. Measure and date of movement on Las Vegas Valley Shear Zone, Clark County, Nevada. Geological Society of America Bulletin 85 (6), 985–989.

Mankinen, E.A., Larson, E.E., Gromme, C.S., Prevot, M., Coe, R.S., 1987. The Steens Mountain (Oregon) geomagnetic polarity transition; 3. Its regional significance. Journal of Geophysical Research 92, 8057–8076.

McFadden, P.L., McElhinny, M.W., 1990. Classification of the reversal test in palaeomagnetism. Geophysical Journal International 103, 725–729.

Metcalf, R.V., Smith, E.I., 1991. Hornblende geobarometry from mid-Miocene plutons; implications regarding uplift and block rotation during Basin and Range extension. Geological Society of America Abstracts with Programs 23 (5), 245.

Onstott, T.C., 1980. Application of the Bingham distribution function in paleomagnetic studies. Journal of Geophysical Research 85 (B3), 1500–1510.

Pike, R.J., Clow, G.D., 1981. Revised classification of terrestrial volcanoes and a catalog of topographic dimensions with new results on edifice volume. U.S. Geological Survey Open File Report OF81-1038, 40pp.

Ron, H., Aydin, A., Nur, A., 1986. Strike-slip faulting and block rotation in the Lake Mead Fault System. Geology 14, 1020–1023.

Sonder, L.J., Jones, C.H., Salyards, S.L., Murphy, K.M., 1994. Vertical axis rotations in the Las Vegas Valley Shear Zone, southern Nevada: Paleomagnetic constraints on kinematics and dynamics of block rotations. Tectonics 13, 769–788.

Thompson, K.G., 1985. Stratigraphy and petrology of the Hamblin–Cleopatra Volcano, Clark County, Nevada. Unpublished MSc thesis, University of Texas at Austin.

Van der Voo, R., 1993. Paleomagnetism of the Atlantic, Tethys, and Iapetus Oceans. Cambridge University Press, Cambridge 411pp.

Watson, G.S., 1956. Analysis of dispersion on a sphere. Royal Astronomical Society Monthly Notices (Geophysical Supplement) 7, 153–159.

Wernicke, B.P., Axen, G.J., Snow, J.K., 1988. Basin and Range extensional tectonics at the latitude of Las Vegas, Nevada. Geological Society of America Bulletin 100, 1738–1757.

Zijderveld, J.D.A.A.C., 1967. Demagnetization of rocks—analysis of results. In: Collinson, D.W., Creer, K.M., Runcorn, S.K. (Eds.). Methods in Palaeomagnetism. Elsevier, Amsterdam, pp. 254–286.